5th IFQMS

The 5th International Forum
on Quantum Metrology and Sensing

PROCEEDINGS

Short Presentation Session for Young Scientists
Part 2: SE-03B

29 November, 2022
Online Conference (Zoom)

Joint Program Session with Quantum Innovation 2022

Proc. 5th IFQMS (The 5th International Forum on Quantum Metrology and Sensing)

Quantum Sensing Track : Short Presentations by Young Researchers

SE-03B. Short Presentations by Young Researchers on SE-01, 04, 06, 07 Topics [5th IFQMS]

*Note: Depending on the program, the order of presentations may change within the same group

All the times in the program are Japan Standard time (GMT+9)

Nov 29 (Tue.)	Session / Presentation	Mentor Chair Co-chair / Presenter	Affiliation	Abstract ID
13:10-14:30	SE-03B-α1. Break-out Session 1			
	Chair	Noriaki Yahata	QST	
	Co-chair	Hidetoshi Kono	QST	
	Structural dynamics of the Mn4CaO5 cluster during the S2-S3 transition in photosystem II	Hongiie Li	Okayama U	SE-03B-α1-01
	Visualization of hydrogen in Photosystem II by high-resolution Cryo-EM analysis	Fusamichi Akita	Okayama U	SE-03B-α1-02
	Pulsed-EPR study for radical reactions with biological anitioxidants utilizing quantum effect of electron spin	Hiroki Hirano	Kanagawa U	SE-03B-α1-03
	Coherent control of radical pair by local optimization theory	Akihiro Tateno	Saitama U	SE-03B-α1-04
	Probing the coherent spin dynamics of radical pairs in weak magnetic field using nanoseconds field switching technique	Ryusei Nozawa	Saitama U	SE-03B-α1-05
	Role of a tyrosine radical in the photoreaction of chicken Cryptochrome 4, a magnetoreceptor candidate molecule	Hiroaki Otsuka	Waseda U	SE-03B-α1-06
	Cavity ring-down measurements by continuous pulse trains for magnetic field effects on transient radical species.	Tsubasa Kimura	Saitama U	SE-03B-α1-07
	Germanium vacancy defects in detonation nanodiamonds for temperature sensing	Fu Haining	Kyoto U	SE-03B-α1-08
	Evaluation of the surface-modified nanodiamond probes by in vivo fluorescence imaging	Koki Okamoto	Tokyo Tech	SE-03B-α1-09
	Detection of heat generation from biological system using double quantum thermometry	Hitoshi Ishiwata	QST	SE-03B-α1-10
	The Anomalous Formation of Irradiation Induced Nitrogen-Vacancy Centers in 5-Nanometer-Sized Detonation Nanodiamonds	Frederick Tze Kit SO	Kyoto U	SE-03B-α1-11
	Microwave antenna architecture for quantitative prediction of ODMR signals	Keisuke Oshimi	Okayama U	SE-03B-α1-12
14:50-16:10	SE-03B-α2. Break-out Session 1			
	Chair	Yoichi Takakusagi	QST	
	Co-chair	Ryoko Araki	QST	
	An Artificial Intelligence Nanopore Platform Detects Omicron SARS-CoV-2 in clinical samples	Kaoru Murakami	Hokkaido U	SE-03B-α2-01
	Non-equilibrium phi4 theory in a Hierarchy: Towards Manipulating Holograms in Quantum Brain Dynamics	Akihiro Nishiyama	Kobe U	SE-03B-α2-02
	Construction of dipeptide-based DNP-NMR molecular probe library focusing on kidney injury mouse model	Yuki Aketa	U Tokyo	SE-03B-α2-03
	Nuclear hyperpolarization of liquid water by using photoexcited triplet electrons in organic nanocrystals	Naoto Matsumoto	Kyushu U	SE-03B-α2-04
	Development of Polarizing Agent with Controlled Electronic Structure for Highly Efficient triplet-DNP	Keita Sakamoto	Kyushu U	SE-03B-α2-05
	DNP-NMR molecular probe for the detection of Dipeptidyl peptidase-4 activity in vivo	Akihito Goto	U Tokyo	SE-03B-α2-06
	Generation of polarized triplet electron spins at solid-liquid interfaces	Reiya Yabuki	Kyushu U	SE-03B-α2-07
	Photoreaction study of a primate blue-light sensitive photoreceptor using vibrational spectroscopy	Yosuke Mizuno	Nagoya Tech	SE-03B-α2-08
	Novel photoisomerization reaction in near-infrared light absorbing enzymerhodopsins	Masahiro Sugiura	Nagoya Tech	SE-03B-α2-09
	Development of a real-time 4D quantum temperature imaging system to measure intercellular thermal diffusivity	Haruka Maeoka	Hiroshima U	SE-03B-α2-10
	Bidirectional neural network and its application to image denoising, super-resolution, and image completion	Kei Majima	QST	SE-03B-α2-11
	Molecular insight into photoactivation mechanism of BLUF protein by QM/MM free energy simulation	Masahiko Taguchi	QST	SE-03B-α2-12

SE-03B-α1-01

Structural dynamics of the Mn_4CaO_5 cluster during the S_2-S_3 transition in photosystem II

Hongjie Li[1], Yoshiki Nakajima[1], Daichi Yamada[2], Kana Hashimoto[1], Minoru Kubo[2,3], So Iwata[3,4], Michihiro Suga[1] and Jian-Ren Shen[1]

[1]*Research Institute for Interdisciplinary Science and Graduate School of Natural Science and Technology, Okayama University, Okayama, Japan*

[2]*Graduate School of Science, University of Hyogo, Hyogo, Japan,*

[3]*RIKEN SPring-8 Center, Hyogo, Japan*

[4]*Department of Cell Biology, Graduate School of Medicine, Kyoto University, Kyoto, Japan*

Introduction

Photosystem II (PSII) catalyzes light-induced water oxidation through the S_i-state cycle at its oxygen-evolving catalyst, a Mn_4CaO_5 cluster. During this process, four electrons and four protons are released from two water molecules, and one di-oxygen molecule is evolved. Pump-probe time-resolved serial femtosecond crystallography (TR-SFX) has been used to capture several intermediate states of PSII, deepening our understanding of the water oxidation reaction. Significantly, a newly inserted oxygen O6 was observed in the vicinity of O5 in the S_3-state before the di-oxygen formation[1,2]. However, the origin of the O6 and the mechanism to incorporate it remain to be elucidated. To address this issue, we analyzed the structural dynamics of PSII during the onset of S_2-S_3 state transition at various time points from nanoseconds to milliseconds after two flashes (2F) illumination using an X-ray free electron laser at SACLA, Japan.

Following the 2nd flash, no difference electron densities was observed within 20 ns. Instead, from 200 ns to 30 µs, paired positive and negative difference densities appeared in the area around Q165 and Y_Z, which was decreased at 200 µs and vanished at 5 ms following the 2nd flash (Fig. 1). Refined models demonstrate that Q165 and Y_Z move in the same direction during 200 ns to 30 µs and restore by 5 ms. These movements can be explained by the oxidation and re-reduction of Y_Z during the S_2-S_3 state transition.

One positive density close to the Ca^{2+} ion, constructed with a water molecule and designated as O6*, appeared during 1 µs to 200 µs and vanished at 5 ms, with the concomitant increase of the O6 density from 30 µs to 5 ms (Fig. 1). We speculate that this water is the origin of O6 and is translocated via the Ca^{2+} ion binding site to the O6 site. Following the insertion of O6, Mn4 and Mn1 move apart from each other, opening the Mn_4CaO_5 cluster and presumably preparing for subsequent di-oxygen release in the next state transition.

These results provide important insights into the molecular mechanism of water oxidation in PSII.

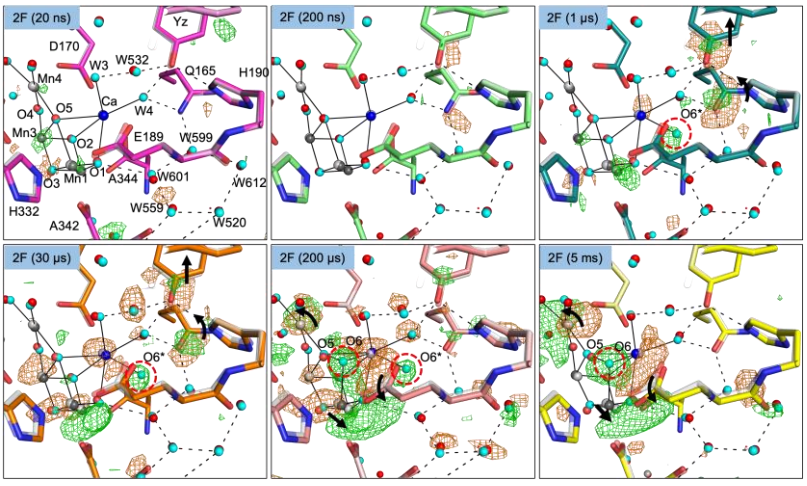

Fig. 1. Structural dynamics around the Mn_4CaO_5 cluster during the S_2-S_3 transitions. Refined structures are superposed with $F^{obs}_{(2F)} - F^{obs}_{(1F)}$ difference density maps contoured at +3.5 (green) and -3.5 (orange) from 20 ns to 5 ms. The 1F structure is in grey and the 2F intermediate structure is colored. Black dot lines depict hydrogen bonds. Black arrows represent structural changes.

Reference

[1]Suga, M. *et al.*, *Nature* **543**, 131-135 (2017)

[2]Suga, M. *et al.*, *Science* **366**, 334-338 (2019)

SE-03B-α1-02

Visualization of hydrogen atoms in Photosystem II by high-resolution Cryo-EM analysis

Fusamichi Akita[1], Radostin Danev[2,3], Yoshiki Nakajima[1], Huaxin Yu[4], Koji Kato[5], Naoyuki Miyazaki[6], and Jian-Ren Shen[1]

[1]*Research Institute for interdisciplinary Science, Okayama University*
[2] *Graduate School of Medicine, The University of Tokyo*
[3]*PRESTO, Japan Science and Technology Agency*
[4]*Microbial Sciences Institute, Department of Microbial Pathogenesis, Yale University*
[5]*Structural Biology Division, Japan Synchrotron Radiation Research Institute*
[6]*Osaka Research Center for Drug Discovery, Otsuka Pharmaceutical Co., Ltd.*
fusamichi_a@okayama-u.ac.jp

Introduction

Photosystem II (PSII) is a membrane protein supercomplex and functions to catalyze light-induced water-splitting, leading to the generation of electrons, protons, and molecular oxygen. PSII consists of 20 protein subunits and several cofactors, chlorophylls, carotenoids, and the oxygen-evolving center (OEC) responsible for splitting water through five intermediate states, S_0, S_1, S_2, S_3, and S_4. The structure of PSII at 1.9 Å resolution was solved in 2011, which revealed that the OEC has a "distorted chair" shape with a Mn_4CaO_5 composition[1]. The structure of PSII without radiation damage at the S_1 state was determined at 1.95 Å resolution using femtosecond X-ray free electron lasers (XFEL)[2]. Subsequently, the S_3 state was analyzed using a time-resolved serial XFEL[3], and the structural transition from S_2 to S_3 was determined using fixed-target XFEL[4]. These studies showed the insertion of an oxygen atom (O6) into the vicinity of O5 in the Mn_4CaO_5 cluster, giving rise to a mechanism of O-O bond formation between O5 and O6. However, there has been little discussion on the protonation states of residues and water molecules as well as hydrogen release pathways, which require high-resolution structural analysis. Recent innovations in cryo-electron microscopy (Cryo-EM) technology have made it possible to achieve high resolutions that may show hydrogen atoms. Here, we analyzed the structure of PSII at 1.45 Å resolution using Cryo-EM. The difference map obtained showed peaks arising from hydrogen atoms around amino acid residues and water molecules. In this presentation, I will discuss the structural analysis of PSII by high-resolution cryo-EM, the protonation states of OEC and the hydrogen atom network.

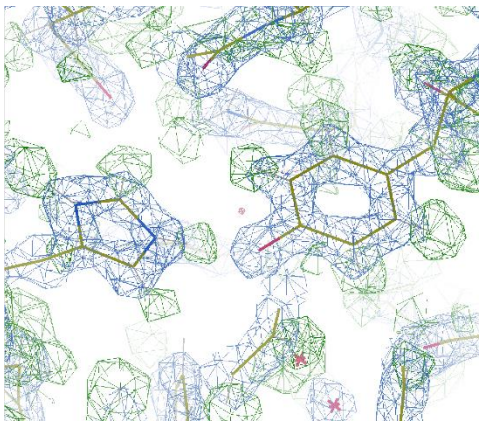

Fig. The Cryo-EM map of PSII at 1.45 Å resolution. The blue and green maps indicate the original Cryo-EM map and the calculated difference map, respectively.

Reference

1. Umena Y., Kawakami K., Shen J.-R., Kamiya N., Crystal structure of oxygen-evolving photosystem II at a resolution of 1.9 Å.*Nature*, 473, 55-60 (2011).
2. Suga M. et al., Native structure of photosystem II at 1.95 Å resolution viewed by femtosecond X-ray pulses. *Nature*, 517, 99-103 (2015).
3. Suga M. et al., Light-induced structural changes and the site of O=O bond formation in PSII caught by XFEL. *Nature*, 543, 131-135 (2017).
4. Suga M.et al., An open-cubane oxyl/oxo mechanism for O=O bond formation in PSII revealed by XFEL.*Science*, 366, 334-338 (2019).

SE-03B-α1-03

Pulsed-EPR study for radical reactions with biological antioxidants utilizing quantum effect of electron spin

Hiroki Hirano[1], Kaito Marumo[1], Ikuo Nakanishi[2], Akio Kawai[1],

[1]*Graduated School of Science, Kanagawa university*

[2]*Institute for Quantum Life Science, Quantum Life and Medial Science Directorate, National Institutes for Quantum Science and Technology*

r201503326@jindai.jp

Introduction

Radicals are important species that are highly reactive and play an important role in biological reactions. Usually, aging and disease of living body are caused by radicals. To protect these problems, there are many biological antioxidants in vivo. The biological antioxidants work to eliminate highly reactive radicals by reacting with them and transform themselves into stable radical species. A large number of studies have been made to determine radical reaction rate constants of biological antioxidants to evaluate radical trapping abilities[1]. What seems to be lacking, however, is the observation in elementary reaction process, particularly in reactions with carbon-centered radicals. For understanding of the radical reactions, it is necessary to discuss them in terms of the kinetics of the elementary reaction process observations.

We have been investigating radical addition reaction mechanisms and rate constants by utilizing time-resolved (TR-) EPR and pulsed-EPR[2]. These methods can observe elementary reaction process owing to their high time resolutions of several 10 ~ 100 ns. The radical reaction rate constants are obtained by measuring the electron spin echo (ESE) decay utilizing pulsed-EPR. The ESE signal is given by the spin wave packet of radicals that are in coherent state. Therefore, the radicals can be selectively observed. In this study, we aim to investigate radical reactions of biological antioxidants by identifying the reaction product radicals and determine radical rate constant of biological antioxidants utilizing these techniques.

Experimental method

TR-EPR measurement was performed to identify the intermediate radicals formed by radical reactions of antioxidants. Radical reaction rate constants of antioxidants were determined by ESE decay measurements. The radicals were generated by photolysis of radical sources such as aromatic ketone compounds. As for the antioxidants, α-tocopherol (α-TocH) and tri-*tert*-butylphenol (TTBP) were used.

Results and Discussion

Fig.1 shows the ESE decays of 2-hydroxypropyl (2Hy-Pr) radical under different α-TocH concentrations. The ESE of the radicals was generated by a conventional Hahn echo pulse sequence with a π/2 pulse and a τ-delayed π pulse, which was initiated at t ns after the laser flash (laser flash – t – π/2 – τ – π – τ – ESE). The decay was obtained by monitoring the ESE signal intensity, S(τ), for series of τ values. The top line is the ESE decay of the 2Hy-Pr radical without antioxidants. The ESE decay rate, $1/T_M^*$, was determined by the exponential decay fitting procedure of the S(τ) profile on the basis of the equation,

$$S(\tau) = S_0 \exp\left(\frac{2\tau}{T_M^*}\right)$$

with S_0 (initial ESE amplitude) and T_M^* as a fitting parameter. Then, the ESE decay measurements were performed with different concentrations of α-TocH (Fig.1). It was found that the $1/T_M^*$ was faster depending on the α-TocH concentration. This is due to the elimination of 2Hy-Pr by the reaction with α-TocH. $1/T_M^*$ of these decays were also determined and the results were plotted against the concentration of α-TocH (Fig.2). The liner relationship was obtained and therefore, the radical reaction rate constant, k, was determined by the liner fitting following the equation,

$$\frac{1}{T_M^*} = \frac{1}{T_M} + k\,[\alpha\text{-TocH}]$$

where $1/T_M$ is the α-TocH -independent the ESE decay rate. The determined k value was (3.2 ± 0.2) ×10^6 M^{-1} s^{-1}. At the conference, we will discuss the reactivity of α-TocH by comparing the rate constant of TTBP.

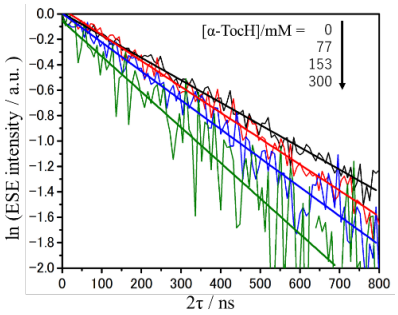

Fig.1 Time profiles of ESE intensity, $S(\tau)$, of 2Hy-Pr under various α-TocH concentrations.

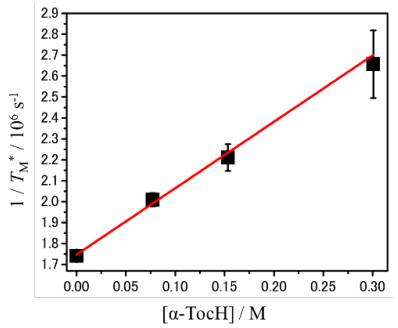

Fig.2 Stern-Volmer type analysis of $1/T_M^*$ of 2Hy-Pr radical versus [α-TocH].

Reference

[1] Packer, J. E., Slater, T. F., and Willson, R. L., *Nature*, 278, 737–738 (1979)

[2] H. Hirano, H. Takahashi, A. Kawai, *J. Phys. Chem. B*, 126, 6074-6082. (2022)

SE-03B-α1-04

Coherent control of radical species by local optimization theory

Akihiro Tateno[1], Kenta Masuzawa[1], Hiroki Nagashima[1], Michihiko Sugawara[2], and Kiminori Maeda[1]

[1]*Graduate School of Science and Engineering, Saitama University*

[2]*Keio Quantum Computing Center, Keio University*

a.tateno.275@ms.saitama-u.ac.jp

Introduction

Design of laser waveforms optimized for reaction control has attracted theoretical and experimental attention[1]. However, it is not easy to realize the designed laser field. In contrast, recent progress of arbitrary wave generator (AWG) enables us to produce the designed radio wave field (RF). Recently, we have shown that it is possible to control the recombination reaction of a radical pair (RP) in high field using radio wave magnetic resonance designed based on the local optimization theory[1,2]. As an example of coherent control, here we show the spin multiplicity control of RP at low fields and the design of optimized AWG pulse that induce selective spin echoes.

Coherent control in local optimization targets a transient state $|f\rangle_L$ that is non-eigenstate of the Hamiltonian at a specific time t_f. In order to produce $|f\rangle_L$ at t_f, it is necessary to calculate the moving target $|\rho_f\rangle_L$ that time-evolves to $|f\rangle_L$. $|\rho_f\rangle_L$ can be calculated by the time reverse Liouville operator as shown by

$$|\rho_f\rangle_L = exp\left\{i\hat{\hat{L}}_0(t_f - t)\right\}|f\rangle_L$$

We have chosen the singlet state and the S_y+S_z states as $|f\rangle_L$ for the reaction control of RPs and the selective spin echo measurement, respectively.

The calculation for the spin multiplicity control was done in a model RP system having one nuclear spin (HFC A=0.5 mT). In low magnetic field, almost all spin states are mixing coherently. We calculated an RF field with the aim of controlling a singlet born RP to singlet state after 1 μs. The FIG.1a shows time-evolutions of the singlet probability in presence and absence of designed RF field. The RF irradiation change the singlet probability at 1 μs after the production of RP from 39 % to 96 %.

As a model system for selective control of spin systems, we used a mixed system of TEMPO (solution) and BDPA (solid) whose stick diagram of the resonance lines is shown in FIG. 1b. In this system, we designed the RF waveform so that the electron spin of TEMPO radical transitions to the S_y state for three hyperfine lines at t =200 ns keeping the electron spin of BDPA in the Sz state. FIG 1c shows that the calculated RF provides the FT-EPR spectrum of selectively excited TEMPO radicals (solid line) whereas the spectrum obtained by composite pulse of three colour RF pulses contains the signal of undesired the other radical (broken line).

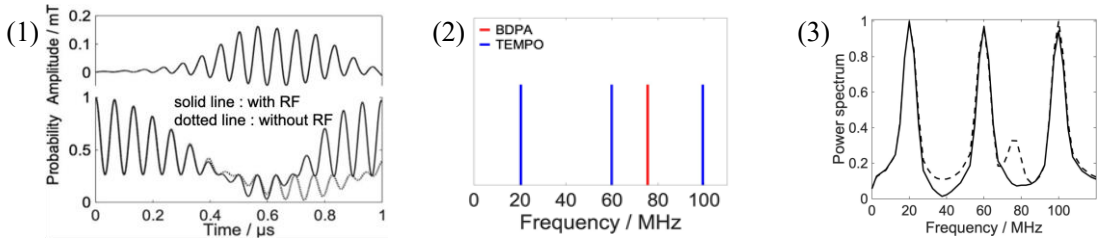

FIG. 1) Upper: Calculated RF, Lower: Time-evolution of singlet probability. 2) Model system 3)Calculated spin echo after optimised pulse(solid line) and after multi-colour pulse(dotted line)

References

[1]M. Sugawara, *J. Chem. Phys.***118(15)**. 6784-6800 (2003).

[2]K. Masuzawa, M. Sato, M. Sugawara, and K. Maeda, *J. Chem. Phys.* **152**, 014301 (2020)

SE-03B-α1-05

Probing the coherent spin dynamics of radical pairs in weak magnetic field using nanoseconds field switching technique

Ryusei Nozawa[1], Taisuke Matuo[1], Hiroki Nagashima[1], Kiminori Maeda[1]

[1]*Department of Chemistry, Graduate School of Science and Technology, Saitama University.*

r.nozawa.939@ms.saitama-u.ac.jp

Introduction

Recent discussions of the mechanism of magnetic sensitivity in animals have focused attention on the spin dynamics of radical pairs in the low-field region and the effects of the magnetic field. The existence of low-field effects in radical pairs is easy to confirm, since the magnetic field effects in radical pairs are in the opposite direction of those in the usual hyperfine coupling and relaxation mechanisms, but there are many theoretical models that are believed to be responsible for the magnetic field effects.[1] Matsuo et al. used nanosecond magnetic field switching techniques for the xanthone-DABCO system in SDS micelle solutions to analyze the behavior of radical pairs at weak magnetic fields and found the decay time of the transient absorption change was extremely short only when the external magnetic field was changed from the peak magnetic field of the low-field effect to zero field.[2] This result suggests that the origin of the low-field effect in this system is not pseudo-normal spin mixing, but coherent due to the breaking of the degenerate electron-nuclear spin state. We also thought we could observe a time equivalent to coherent low-field effect generation by applying nanosecond magnetic field switching techniques. Based on these, the nanosecond magnetic field switching technique was further applied in this study to four more magnetic fields exhibiting low-field effects to zero field to probe the coherent low-field effect generation process.

Method・Result

MARY spectra in the low-field region obtained in SDS micellar solutions of xanthone and DABCO are shown in FIG 1[a]. Transient absorption changes associated with magnetic field switching from four low magnetic fields(1.5, 1.1, 0.7, 0.4 mT) to zero magnetic field were monitored and their post-laser delay time dependence plotted. Experimental results on the curve of $t \approx h/2g\mu_B B_0$ as shown FIG1[b]. Comparing this result with the time evolution of the Singlet-like magnetic field effect by the one-nucleus spin model, it reflects the most prominent time of the coherent onset of the low-field effect due to the breaking of the degeneracy of the electron-nucleus spin state by the Zeeman energy. This indicates that the present method captures the generation of the low-field effect due to the breaking of the degeneracy in time. However, some other systems do not exhibit such ideal behavior and don't reflect the coherent rise time. This indicates the possibility of the influence of decoherence of spin systems, mechanisms of low-field effects other than degenerate breaking, and so on.

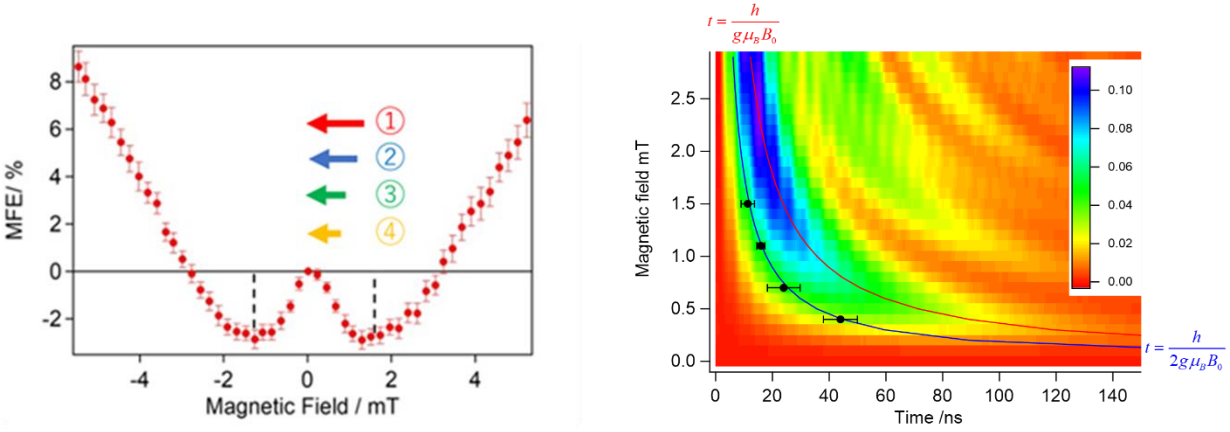

FIG.1. [a]Experimental results of MARY spectra of the Xanthone-DABCO system and the scheme for changing the magnetic field. [b] Calculation results magnetic field effects of Singlet in the one-nuclear spin, and the result of inverse field switching.

Reference

[1] [1]Maeda, K. et al., *Nature*, 452,387-390(2008).
[2] [1]Matuo.T., *Master thesis*(2018).

SE-03B-α1-06

Role of a tyrosine radical in the photoreaction of chicken Cryptochrome 4, a magnetoreceptor candidate molecule

Hiroaki Otsuka[1], Ryosuke Miyake[1], Keiko Okano[1], Yasushi Imamoto[2], and Toshiyuki Okano[1]

[1]*Department of Electrical Engineering and Bioscience, School of Advanced Science and Engineering, Waseda University*

[2]*Department of Biophysics, Graduate School of Science, Kyoto University*

o1.2t5.8tt21.tf@ruri.waseda.jp

Introduction

Some animals have the ability of magnetoreception [1]. Interestingly, the magnetoreception of birds and insects is driven by light. As a possible mechanism of the light-dependent magnetoreception, "Radical pair mechanism (RPM)" has been proposed, in which the magnetosensitive bifurcation of reaction of two entangled radicals (radical pair) formed by photoexcitation is used [2]. The magnetic sensor in RPM would have the light-sensitivity and the ability of radical formation, and cryptochromes (CRYs) are considered to be candidates for the magnetoreceptor. Our previous study revealed the ability of photoreception via flavin adenine dinucleotide chromophore (FAD) and radical formation of CRY4 in the chick retina [3–5]. The spectroscopic analysis of the transient reaction of chicken CRY4 (cCRY4) identified a formation of FAD anion radical ($FAD^{\bullet-}$) upon light absorption, which was reacted into bifurcated reaction of oxidation or protonation. Interestingly, a neutral tyrosine radical ($Tyr\text{-}O^{\bullet}$) like spectrum was detected with the formation of $FAD^{\bullet-}$ and it decayed along with the protonation of $FAD^{\bullet-}$ [6]. According to RPM, magnetosensitive reaction of bifurcation to reduction and oxidation is expected to a key step. Although the detail role and the site of $Tyr\text{-}O^{\bullet}$ formation are unknown, $Tyr\text{-}O^{\bullet}$ could play an important role in the bifurcation.

In this study, we aim to identify the site of $Tyr\text{-}O^{\bullet}$ formation and elucidate the role of $Tyr\text{-}O^{\bullet}$ in the photoreaction of cCRY4 by comparing the photoreaction of cCRY4 tyrosine mutant with that of wild-type cCRY4.

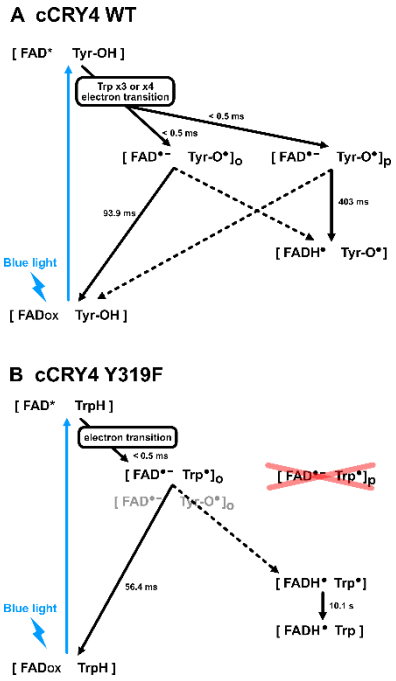

FIG. 1. Reaction model of cCRY4 WT and cCRY4 Y319F (A) $FAD^{\bullet-}$ binding cCRY4 is bifurcated into oxidation form and protonation form. $Tyr\text{-}O^{\bullet}$ decays as $FAD^{\bullet-}$ oxidizes. (B) Almost $FAD^{\bullet-}$ oxidizes in cCRY4 Y319F, and $Trp^{\bullet}$ is formed instead of $Tyr\text{-}O^{\bullet}$.

Method

Tyr319 is an amino acid locating near the fourth tryptophan that constitutes a putative electron-transfer pathway called Trp-tetrad in cCRY4, and it was mutated to phenylalanine (F). Wild-type and Y319F mutant of recombinant cCRY4 were expressed by yeast expression system and purified by GST-tag-based purification system. Steady-state photoreactions and their efficiencies were analyzed using double beam spectroscopy (UV-2450). Transient reactions of each sample were measured by laboratory-built, time-resolved spectrophotometry system.

Results and discussion

The chromophore FAD in the dark-state of cCRY4 is oxidized (FAD_{OX}). Blue light irradiation reduces the FAD_{OX} to $FAD^{\bullet-}$, a part of which is immediately (subsecond order) protonated to a neutral radical form ($FADH^{\bullet}$). Quantum yield of $FAD_{OX} \rightarrow FADH^{\bullet}$ in cCRY4 WT was 16%, while that in cCRY4 Y319F decreased to 6.0%. As reported previously, cCRY4 WT showed $FAD^{\bullet-}$ formation immediately after photoexcitation (< 0.5 ms), followed by bifurcation to fast (≈ 100 ms) oxidation ($FAD^{\bullet-} \rightarrow FAD_{OX}$) and slow (≈ 400 ms) protonation ($FAD^{\bullet-} \rightarrow FADH^{\bullet}$), the former of which was accompanied by decay of $Tyr\text{-}O^{\bullet}$ (FIG. 1A). In contrast, most of the $FAD^{\bullet-}$ was oxidized in cCRY4 Y319F, and noticeably, spectra resembling tryptophan neutral radicals ($Trp^{\bullet}$) instead of $Tyr\text{-}O^{\bullet}$ were observed (FIG. 1B).

The observation of $Trp^{\bullet}$-like spectra in cCRY4 Y319F is consistent with the idea that Tyr319 donates electron to FAD via Trp tetrad. The suppression of the $FAD^{\bullet-}$ protonation in cCRY4 Y319F suggests a possible role of $Tyr\text{-}O^{\bullet}$ in the protonation.

Reference

[1]R. Wiltschko and W. Wiltschko, *Adv. Exp. Med. Biol.* 739, 126 (2012); [2]T. Ritz, S. Adem, and K. Schulten, *Biophys. J.* 78, 707 (2000); [3]Y. Kubo, M. Akiyama, Y. Fukada, and T. Okano, *J. Neurochem.* 97, 1155 (2006); [4]R. Watari, C. Yamaguchi, W. Zemba, Y. Kubo, K. Okano, and T. Okano, *J. Biol. Chem.* 287, 42634 (2012); [5]H. Mitsui, T. Maeda, C. Yamaguchi, Y. Tsuji, R. Watari, Y. Kubo, K. Okano, and T. Okano, *Biochemistry* 54, 1908 (2015). [6]H. Otsuka, H. Mitsui, K. Miura, K. Okano, Y. Imamto, and T. Okano, *Biochemistry* 59, 3615 (2020).

SE-03B-α1-07

Cavity ring-down measurements by continuous pulse trains for magnetic field effects on transient radical species.

Tsubasa Kimura[1] and Kiminori Maeda[1]

[1]*Department of Chemistry, Graduated school of Science and Engineering, Saitama University*

t.kimura.485@ms.saitama-u.ac.jp

Introduction

The magnetic field effect (MFE) measurements of photo-generated radical pairs in photochemical reactions fundamentally need very high sensitivity and long acquisition with many light pulse irradiations. The degradation due to the multiple pump pulse irradiations is a difficult concern when we apply to precious biological samples. Previously, the sensitivity problem was solved with pump-probe type cavity ringdown (CRDS) method [1], which boosts the effective optical path length using optical cavity. If we compared the CRDS with the cavity enhanced absorption spectroscopy (CEAS) [2], the CRDS on transient absorption (TA) measurements has advantageous aspects: 1) free from correction of the wavelength dependent cavity enhancement, 2) free from the fluctuations of the probe beam, 3) clear estimation of the time resolution.

Here we developed a new CRDS technique named super-CRDS (SCRDS) [3], which is sequential CRDS measurements using a pulse train of a super continuum source (SC source). SCRDS allows us to measure the absorptions at many delay times with 200 ns interval (5 MHz). Therefore, we can get the transient absorption (TA) time trace by a single excitation simultaneously. This fact dramatically reduces the number of excitation light irradiations, keeping the sensitivity as same as pump-probe CRDS.

Method

The TA at 500~600 nm and its magnetic field effect were measured by SCRDS technique. The mixed aqueous solution of FMN 50 μM and HEWL 200 μM, 40 mL was flown from a syringe pump to a sample cell (200 μL volume and 1 mm optical length). The CRDS signal is penetrated from the back side of the cavity mirror and monitored by a photomultiplier tube. The CRD signals are fit by a single exponential function for every delay times. The transient absorbances ΔA per single pass of the probe light can be calculated by the lifetime of the signal τ and that at the negative delay time τ_0. The TA was measured in the field range from 0 to 20 mT. Pulsed magnetic fields, whose duration is 1.8 ms, were synchronized with the excitation pulse laser. The flat region of the magnetic field in time was used for the TA measurements. In the MFE measurement, the absorption was measured while the magnetic field was varied by 2 mT, and the absorption from 10 to 90 μs was averaged to obtain the magnetic field effect at each magnetic field. This process was repeated 200 times at each magnetic field.

Results

The intensity of the excitation light was adjusted to be comparable to that of Ref [1]. FIG. 1 is a plot of TA time profiles, and FIG. 2 is a plot of MFE measurement. SCRDS requires only one-tenth of the number of shots, (200 shots), to measure the TA for a single magnetic field intensity, and the error can be suppressed to ±0.25 %.

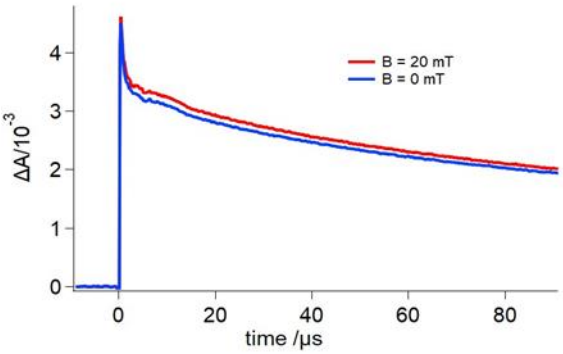

FIG. 1. Time-resolved transient absorption signal in the system of FMN 50 μM and HEWL 200 μM. The signal obtained by 100 shots laser excitation is averaged.

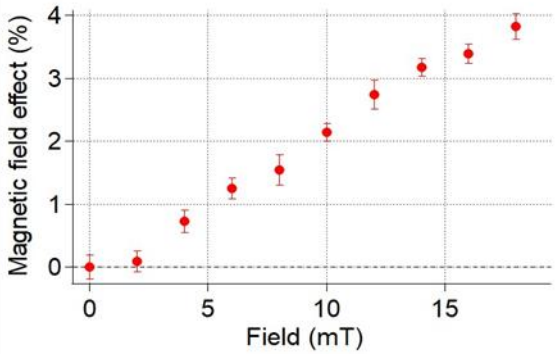

FIG. 2. Magnetic field effect using SCRDS in the system of FMN 50 μM and HEWL 200 μM. 200 shots averaged per points.

Acknowledgements: This work was supported by MEXT Q-LEAP Grant Number JPMXS0120330644

References: [1] Maeda, K *et al.*, *J. Am. Chem. Soc.*, **133,** 17807–17815 (2011).
[2] Neil, S. R. T *et al. J. Phys. Chem.* B, **118,** 4177-4184(2014).
[3] Japan Patent 2022- 7803.

SE-03B-α1-08

Germanium Vacancy Defects in Detonation Nanodiamonds for Temperature Sensing

Haining Fu[1], Masanori Fujiwara[1], Izuru Ohki[1], Ming Liu[2], Akihiko Tsurui[2], Taro Yoshikawa[2], Masahiro Nishikawa[2], and Norikazu Mizuochi[1]

[1]*Institute for Chemical Research, Kyoto University*

[2]*Daicel Cooperation*

fu.haining.82r@st.kyoto-u.ac.jp

Introduction

Group IV color centers such as silicon-vacancy center (SiV) and germanium-vacancy center (GeV) in nanodiamonds (NDs) are promising candidates for all-optical nanoscale thermometry. Because these defects have sharp zero phonon lines (ZPLs) and the ZPL peak wavelength changes depending on local temperature. For live-cell application, NDs should be smaller than 30 nm to avoid non-invasive methods. However, the minimum size of NDs concluding group IV color centers as temperature sensors reported was 200 nm [1]. This motivated us to synthesize NDs by detonation method, which is suitable for the mass production of NDs in smaller size. In 2020, we reported the first synthesis of SiV-containing detonation nanodiamonds (SiV-DNDs) [2]. Then, we performed all-optical thermometry with SiV-DNDs in an average size of 20 nm. This is the smallest size applied for thermometry using color-center-containing NDs [3].

Compared to SiV center, GeV center shows higher quantum efficiency, and its ZPL peak wavelength is 100 nm shorter than SiV center, make it a good candidate for temperature sensing. GeV-containing detonation nanodiamonds (GeV-DNDs) has been synthesized successfully according to the recent report [4]. And in our current study, we focus on the temperature sensing of GeV-DNDs, evaluated their PL spectrum response according to temperature. GeV center combining SiV center is suitable for multi-color imaging application and local temperature measurements of live-cell organelles.

Methods & Results

After the detonation of explosives with Ge dopant, our sample was processed by purification, dispersion, surface modification, and ultracentrifugation. Supernatant and suspension were collected as different samples. In addition, the sediment was also collected and dispersed into pure water as another sample. Each sample was dropped on a coverslip, natural drying in the air atmosphere. A thermoplate is set to control the sample temperature. Each sample were observed and taken photoluminescence (PL) image by a homebuilt confocal microscope.

Both the supernatant and suspension samples showed weak GeV centers' ZPL signals at around 602 nm, and a strong PL background signal from DND itself has been observed. In the sediment sample, however, we found a strong ZPL signal from some bright spots in PL image (Fig. 1(a)). These bright spots may be GeV-DND aggregations or large GeV-DND particles. At these spots, we confirmed that the ZPL peak wavelength (λ) linearly red-shifted with increasing temperature (T) (Fig. 1(b)). The slope $\Delta\lambda/\Delta T$ is an indicator of the temperature response and the average value is 0.009 nm/K, which agrees with the GeV center ensemble in a bulk diamond (0.008 nm/K) [5]. The particle distribution is investigated by transmission electron microscope image. The average particle size is 20 nm, much smaller than the reported GeV-NDs for thermometry application (400 nm) [6]. Finally, we measured and calculated the temperature sensitivity (η_T), which defined as the temperature deviation (σ_T) per unit integration time (1s). As an example, a temperature sensitivity as 1.9 K $Hz^{-1/2}$ measured at a bright spot shows in Fig. 1(c), means that a sub-Kelvin temperature change can be measured in 10 seconds.

This work is supported by MEXT Q-LEAP (No. JPMXS0120330644).

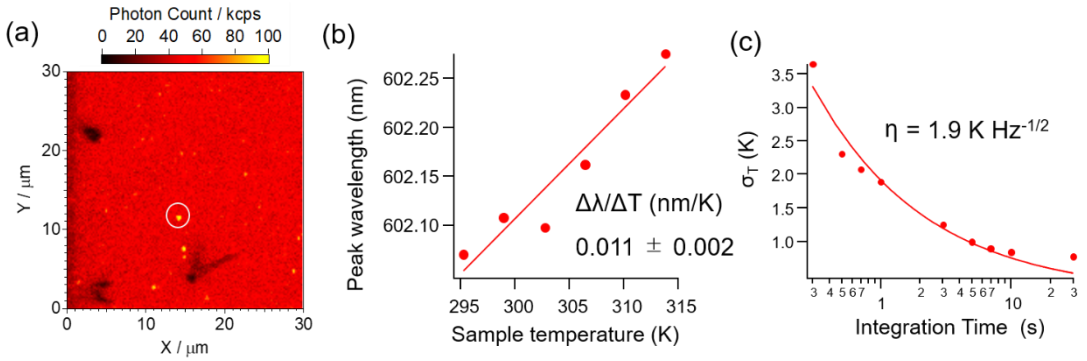

Figure 1 (a) PL image of the GeV-DND sediment sample. (b) and (c) Temperature dependence and temperature sensitivity measurements at the bright spot depicted in a white circle in (a).

Reference

[1] C. T. Nguyen, et al., *Appl. Phys. Lett.* 112, 203102 (2018). [2] Y. Makino, et al., *Diam. Relat. Mater.* **112**, 108248 (2021). [3] M. Fujiwara, et al., *Carbon*, **198**, 57 (2022). [4] Y. Makino, et al., *Diam. Relat. Mater.* **130**, 109493 (2022) [5] S. Blakley, et al., *ACS Photonics*, **6**,1690 (2019). [6] T. T. Tran, et al., *Sci. Adv.* **5** eaav9180 (2019)

SE-03B-α1-09

Evaluation of the surface-modified nanodiamond probes by *in vivo* fluorescence imaging

Koki Okamoto[1], Masaya Muto[1], Tetsuya Kadonosono[1], Kiichi Kaminaga[2], Ryuji Igarashi[2], and Shinae Kizaka-Kondoh[1]

[1]*School of Life Science and Technology, Tokyo Institute of Technology*

[2]*Institute for Quantum Life Science, National Institutes for Quantum Science and Technology*

okamoto.k.am@m.titech.ac.jp

Introduction

In recent years, fluorescent nanodiamond have attracted attention as a novel *in vivo* imaging probe[1]. Nitrogen-vacancy centers in nanodiamond have electrons whose quantum state (such as spin resonance frequencies) change according to changes in the surrounding environment. This variation of quantum state can be used to develop environmentally responsive sensor probes[2, 3]. Tumors have a unique and complex microenvironment characterized by hypoxia[4], which is closely associated with treatment resistance and malignant progression, making it important therapeutic targets. Early detection of tumor hypoxia is expected to contribute to the improvement of cancer treatment.

Our goal in this research is to develop nanodiamond imaging probes that can detect hypoxia in tumors with high sensitivity . Here, we take full advantage of the excellent photostability of fluorescent nanodiamonds, to perform fundamental *in vivo* evaluations of 50-100 nm surface-modified diamond nanoparticles, which are the basic for creating hypoxia probes. We evaluated their fluorescence sensitivity upon *in vivo* administration (intratumoral, subcutaneous, and intravenous) in mice.

Polyglycerol hydrophilically modified 100-nm nanodiamond particles were found to be the most sensitive for fluorescence detection among the particles evaluated, and thus will be used as a base material to create sensor probes that detects hypoxic cells using the cellular oxygen sensor function. Such probes are expected to contribute to early detection of hypoxic diseases including malignant tumors.

This work was supported by MEXT Q-LEAP Grant Number JPMXS0120330644.

Tables and Figures

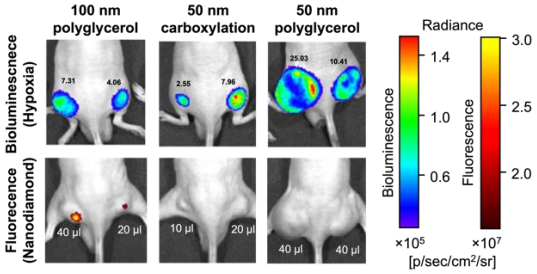

FIG. 1. Representative images of mice with hypoxic tumors (top: bioluminescence) and nanodiamond particles injected into tumor (bottom: fluorescence).

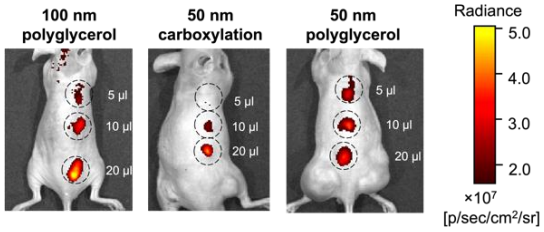

FIG. 2. *In vivo* fluorescence image of subcutaneously injected surface-modified nanodiamond particles.

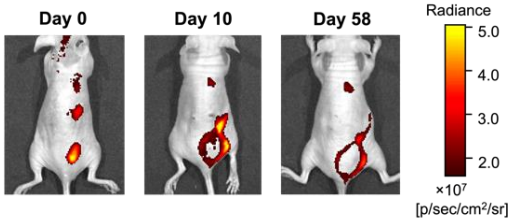

FIG. 3. *In vivo* fluorescence image of 100-nm nanodiamond particles with polyglycerol hydrophilic modification at the indicated time points after subcutaneous injection of the particles.

Reference

[1]M. H. Alkahtani et al., *Nanophotonics*, 7, 1423-1453 (2018)

[2]M. Fujiwara et al., *Sci. Adv.*, 6, 37 (2020).

[3]T. Fujisaku et al., *ACS Nano*, 13, 11726-11732 (2019)

[4]V. Petrova et al., *Oncogenesis*, 7, 10 (2018)

SE-03B-α1-10

Detection of heat generation from biological system using double quantum thermometry

Hitoshi Ishiwata[1], Kano Suzuki[2], Kiichi Kaminaga[1], Takeshi Murata[2], Ryuji Igarashi[1]

[1]QST, Institute for Quantum Life Science,

[2]Graduate School of Science and Membrane

Protein Research and Molecular Chirality Research Centers,

Chiba University

ishiwata.hitoshi@qst.go.jp

Introduction

The NV center in a diamond is a quantum sensor with exceptional quality for highly sensitive thermometry. For quantification of heat generation from biological system, thermometry technique that allows to quantify accuracy and precision of temperature is necessary. While many biological applications have been demonstrated by detection of CW ODMR spectrum from NV center, it is difficult to quantify accuracy and precision of temperature measurement from peak fitting of CW ODMR spectrum. In this talk, we utilized all three energy levels |0>, |±1> of NV center to perform Double Quantum Thermometry for highly sensitive and accurate measurement of temperature. Advantage of biological heat detection using double quantum thermometry will be discussed in the talk.

Result

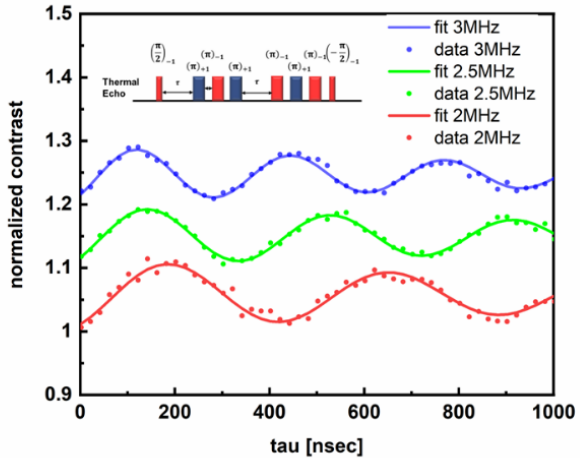

FIG. 1. Double Quantum thermometry using NV center in diamond.

FIG.1 shows typical result of Double Quantum Thermometry by Thermal Echo measurement using NV center in diamond. The energy difference between the bright |0⟩ and dark |± 1⟩ states were observed as an oscillation in the Thermal Echo signal. Inset of Figure 1 shows pulse sequence used for Thermal Echo measurement.

Change in oscillation frequency of Thermal Echo measurement was observed for different value of applied microwave frequency. As difference between applied frequency and D(T) changed from 2 MHz, 2.5 MHz, 3 MHz, oscillation was observed at frequency of 2MHz, 2.5MHz, 3MHz respectively. Analysis of oscillation frequency showed temperature precision of 0.3K, demonstrating sub-degree temperature precision for measurement of biological temperature. Application of quantum thermometry with high precision will be discussed in the talk.

Reference:

This research was supported by MEXT Quantum Leap Flagship Program (MEXT Q-LEAP) Grant Number JPMXS0120330644.

SE-03B-α1-11

5The Anomalous Formation of Irradiation Induced Nitrogen-Vacancy Centers in 5-Nanometer-Sized Detonation Nanodiamonds

Frederick T.-K. So[1,2,3], Alexander I. Shames[4], Daiki Terada[2,3], Takuya Genjo[2,3], Hiroki Morishita[1], Izuru Ohki[1], Takeshi Ohshima[5], Shinobu Onoda[5], Hideaki Takashima[6], Shigeki Takeuchi[6], Norikazu Mizuochi[1], Ryuji Igarashi[3,7], Masahiro Shirakawa[2,3*], Takuya F. Segawa[2,8*]

[1]*Institute for Chemical Research, Kyoto University*
[2]*Department of Molecular Engineering, Graduate School of Engineering, Kyoto University*
[3]*Institute for Quantum Life Science, National Institutes for Quantum and Radiological Science and Technology*
[4]*Department of Physics, Ben-Gurion University of the Negev, Israel*
[5]*Takasaki Advanced Radiation Research Institute, National Institutes for Quantum Science and Technology*
[6]*Department of Electronic Science and Engineering, Kyoto University*
[7]*National Institute for Radiological Sciences, National Institutes for Quantum Science and Technology*
[8]*Laboratory for Solid State Physics, ETH Zurich, Switzerland*
so.kit.58a@st.kyoto-u.ac.jp

Introduction

Nanodiamonds containing negatively charged nitrogen-vacancy (NV^-) centers are versatile room-temperature quantum sensors in a growing field of research. Yet, knowledge regarding the NV^- formation mechanism in very small particles is still limited. This study focuses on the formation of the smallest NV^--containing diamonds, 5 nm detonation nanodiamonds (DNDs). As a reliable method to quantify NV^- centers in nanodiamonds, half-field signals in electron paramagnetic resonance (EPR) spectroscopy are recorded. By comparing the NV^- concentration with a series of nanodiamonds from high-pressure high-temperature (HPHT) synthesis (10–100 nm), it is shown that the formation process in 5 nm DNDs is unique in several aspects. NV^- centers in DNDs are already formed at the stage of electron irradiation, without the need for high-temperature annealing, an effect related to the very small particle size. Also, the NV^- concentration (in atomic ratio) in 5 nm DNDs surpasses that of 20 nm-sized nanodiamonds, which contradicts the observation that the NV^- concentration generally increases with particle size. This can be explained by the 10 times higher concentration of substitutional nitrogen atoms in the studied DNDs ([$N_S \approx 1000$ ppm]) compared to the HPHT nanodiamonds ([$N_S \approx 100$ ppm]). Upon electron irradiation at a fluence of 1.5×10^{19} e^-/cm^2, DNDs show a 12.5-fold increment in the NV^- concentration with no sign of saturation reaching 1 out of about 80 DNDs containing an NV^- center. These findings can be of interest for the creation of defects in other very small semiconductor nanoparticles beyond NV-nanodiamonds as quantum sensors.

This work was supported by MEXT Q-LEAP Grant Number JPMXS0120330644 & JPMXS0118067395, KAKENHI (Grants 20H00453, 18K19297 and 21H04444)

Method

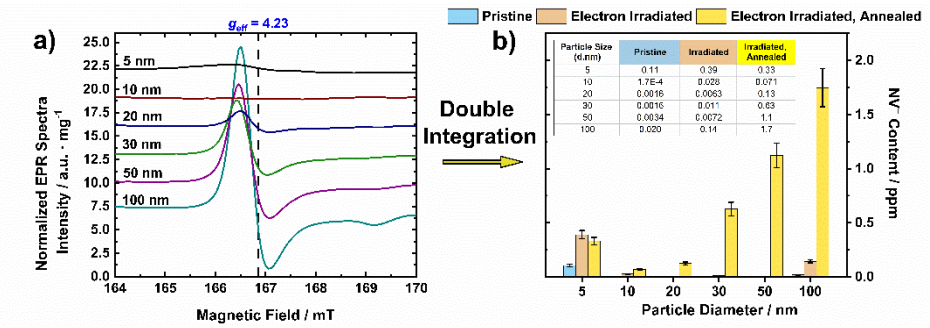

Figure 1. (a) Continuous-wave HF EPR spectra (ν = 9.87* GHz) of electron-irradiated (2 MeV, 5×10^{18} e^-/cm^2) NDs with different particle sizes after high-temperature annealing. The double integral of the signal at g_{eff} = 4.23 provides the NV^- concentration. (b) A summary graph of NV^- content (ppm, in units of atomic ratio) in NDs of different sizes, measured via the HF EPR technique. Blue bars are the pristine NDs, orange bars are the electron-irradiated NDs, and yellow bars are the electron-irradiated and subsequently annealed NDs (derived from the g_{eff} = 4.23 signal in the EPR spectrum of panel a). Electron irradiation was conducted with 2 MeV electrons at a fluence of 5×10^{18} e^-/cm^2. Annealing was performed at 800 °C in vacuum for 2 h. All samples were boiling acid treated at 130 °C for 3 days to remove Fe^{3+} impurities, which overlap with the HF EPR NV^- signal. Inset table shows the corresponding NV^- concentrations in ppm. Errors in NV^- concentration do not exceed ±15%.

SE-03B-α1-12

Microwave antenna architecture for quantitative prediction of ODMR signals

Keisuke Oshimi[1*], Masazumi Fujiwara[1]

[1]*Grad. Sch. Natural Science and Technology, Okayama University*

**pcfw97je@s.okayama-u.ac.jp*

Introduction

Quantum sensing with fluorescent nanodiamonds (NDs) containing nitrogen-vacancy (NV) centers is performed under the fluorescence microscope with microwave irradiation. It reads a modulation of optically detected magnetic resonance (ODMR) of electron spins of NV centers. This technique and the low cytotoxicity and biocompatibility of NDs enable to measure physical quantities inside biological samples, such as electric field, magnetic field, and temperature. So far, several antenna structures have been developed for microwave excitation and used in biological research [1-3]. Recently, we reported a glass-based antenna device having millimeter-scale area of microwave irradiation [4]. In this work, we demonstrate the quantitative prediction of the ODMR on our antenna devices, by thoroughly studying the relationship between the antenna properties and ODMR contrast.

Method

We quantitatively predict ODMR contrast on the glass surface of the antenna chip device developed for ODMR measurements in biological samples (FIG. 1(a)). As shown in FIG. 1(b), we first simulated the microwave magnetic field ($|\boldsymbol{B}|$) in the ODMR measurable area (sample detection area) by numerical simulation based on the finite element method, considering the microwave reflection and transmission of chip devices and microwave components (cables, RF switches, and amplifier). We next converted the simulated $|\boldsymbol{B}|$ to ODMR contrast of NDs using a theoretical equation based on rotational Bloch equations [5]. For the comparison of this theoretical ODMR with the experimental results, we overlaid the theoretical curve, as shown in FIG. 1(c). We found theoretical results closely matched the experimental results, which indicates experimental ODMR measurements are predictable by the numerical simulation at the stage of design development. In the presentation, we explain about the development methodology, and the future biological application of ND-based quantum sensing.

This work was supported by the Nanotechnology Platform Project (Nanotechnology Open Facilities in Osaka University) of MEXT (JPMXP09F21OS0055), JSPS-KAKENHI (19K21935, 20H00335, 20KK0317), AMED (JP21zf0127004), JST (JPMJMI21G1), the MEXT-LEADER program, the Mazda Foundation, and Osaka City University Strategic Research Grant 2017–2020, MEXT Quantum Leap Flagship Program (MEXT Q-LEAP, JPMXS0120330644).

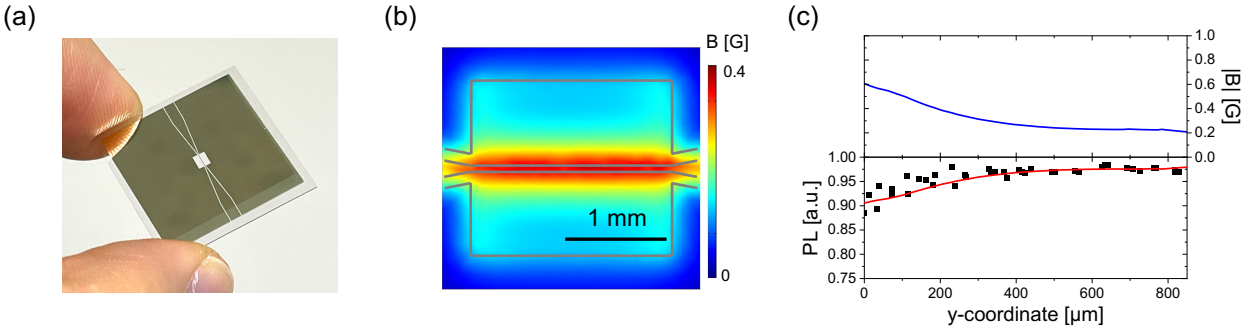

FIG. 1 (a) Photograph of an antenna chip device. (b) The computed spatial distribution of |B| at 2.87 GHz on the chip surface. (c) Position dependence of the simulated |B| (top; blue line) and measured ODMR depth (bottom; black squares) with the line calculated from the simulated |B| (bottom; red line).

Reference

[1]Yukawa et al., Nanoscale Adv., **2**, 1859 (2020). [2]J. Choi et al., PNAS, **117**, 14636 (2020). [3]R. Igarashi et al., J. Am. Chem. Soc., **142**, 7542 (2020). [4] Oshimi, Nishimura, Matsubara, Tanaka, Shikoh, Zhao, Zou, Komatsu, Ikado, Takezawa, Kage-Nakadai, Izutsu, Yoshizato, Morita, Tokunaga, Yukawa, Baba, Teki and Fujiwara, Lab Chip, **22**, 2519 (2022). [5]A. Dréau et al., Phys. Rev. B, **84**, 195204 (2011).

SE-03B-α2-01

An Artificial Intelligence Nanopore Platform Detects Omicron SARS-CoV-2 in clinical samples

Kaoru Murakami[1,2], Shimpei Kubota[1,2], Keiichiro Akabane[1], Kumiko Tanaka[1], Rigel Suzuki[3], Yuta Shinohara[1], Hiroyasu Takei[4], Shigeru Hashimoto[1], Yuki Tanaka[2], Shintaro Hojyo[1,2], Kazuki Sato[1,6], Yuichi Kojima[1,6], Masateru Taniguchi[5*], and Masaaki Murakami[1,2,12*]

1) Molecular Psychoimmunology, Institute for Genetic Medicine, Graduate School of Medicine, Hokkaido University, Sapporo 060-0815, Japan
2) Group of Quantum immunology, Institute for Quantum Life Science, National Institute for Quantum and Radiological Science and Technology (QST), Chiba 263-8555, Japan
3) Department of Microbiology and Immunology, Graduate School of Medicine, Hokkaido University, Sapporo, 060-0815, Japan.
4) Aipore Inc., 26-1 Sakuragaokacho, Shibuya, Tokyo 150-8512, Japan.
5) The Institute of Scientific and Industrial Research, Osaka University, Ibaraki, 567-0047, Osaka, Japan.
6) Department of Hematology, Faculty of Medicine, Hokkaido University, Sapporo, 060-8638, Japan

Abstract

We recently reported a highly accurate, cost-effective artificial intelligence nanopore platform (AI-nanopore platform) to detect coronaviruses, including Wuhan SARS-CoV-2 within five minutes. We here show that this platform can further distinguish SARS-CoV-2 alfa, beta, gamma, delta, and omicron variants. Moreover, it identified mutated Wuhan SARS-CoV-2 expressing the spike proteins of the delta and omicron variants. Furthermore, we identified the omicron variant with a sensitivity of 100% and specificity of over 94% in saliva specimens isolated from COVID-19 patients, which is the similar and/or better values to RT-PCR. Importantly, AI-nanopore platform can identify even low concentrations of omicron variants with both sensitivity and specificity of over 95% in saliva specimens, which had more than 30 Ct values of RT-PCR analysis and are hard to be evaluated by RT-PCR, suggesting that the platform has an advantage over RT-PCR analysis. Thus, this AI-nanopore platform may be an effective diagnostic tool for emerging infectious pathogens including SARS-CoV-2 in clinical situation.

Rationale:

We recently reported an artificial intelligence (AI)-nanopore platform that enables testing for Wuhan SARS-CoV-2 with high sensitivity and specificity. However, which parts of SARS-CoV-2, whether mutated SARS-CoV-2 variants, or clinical samples with low concentration of virus are recognized by the AI-nanopore platform are unknown.

Objectives:

To investigate these three questions.

Methods:
We analyzed cultured SARS-CoV-2 alpha, beta, gamma, delta, and omicron variants using an improved AI-nanopore platform. To identify the specific SARS-CoV-2 structures detected by the platform, we prepared mutated Wuhan variant SARS-CoV-2 expressing the spike proteins of the delta or omicron variants. Additionally, we analyzed 241 saliva samples with omicron variants collected from 132 infected and 109 uninfected people based on RT-PCR results using the platform.

Measurements and Main Results:
The platform distinguished cultured SARS-CoV-2 the five variantsand the mutated Wuhan variant, suggesting the platform's sensitivity for the spike protein. Furthermore, it identified omicron SARS-CoV-2 with a sensitivity of over 100% and specificity of over 94% from saliva specimens isolated from COVID-19 patients. Moreover, the platform can identify even low concentrations of omicron variants with both sensitivity and specificity of over 95% in saliva specimens, which are hard to be evaluated by RT-PCR.

Conclusions:
The AI-nanopore platform is an effective diagnostic tool for SARS-CoV-2 variants in clinical samples even with low concentration virus.

Keywords: COVID-19 diagnosis, AI-nanopore, SARS-CoV-2 variants

SE-03B-α2-02

Non-equilibrium ϕ^4 theory in a Hierarchy: Towards Manipulating Holograms in Quantum Brain Dynamics

Akihiro Nishiyama[1], Shigenori Tanaka[1] and Jack A. Tuszynski[2]

[1]Graduate School of System Informatics, Kobe University, 1-1 Rokkodai, Nada-ku, Kobe, 657-8501, Japan
[2]Department of Oncology, University of Alberta, Cross Cancer Institute, Edmonton, Alberta, Canada T6G 1Z2

anishiyama@people.kobe-u.ac.jp

Introduction

We describe non-equilibrium ϕ^4 theory in a hierarchical manner in order to develop a method for manipulating coherent fields as a toy model of introducing control into Quantum Field Theory (QFT) of the brain, which is called Quantum Brain Dynamics (QBD). We begin with the Lagrangian density of ϕ^4 model, and derive the Klein--Gordon equation of coherent fields with a damping term as an input--output equation proposed in areas of morphological computation or reservoir computing. Our analysis is extended to QFT in a hierarchy representing multiple layers covering cortex in a brain. We find that the desired target function is achieved via time-evolution in the Klein--Gordon Eqs. in a hierarchy of numerical simulations when a signal in both the input and output prevails over noise in the intermediate layers. Our approach will be applied to control coherent fields in the systems (in a hierarchy) described in the QFT framework, with potential applications allowing to manipulate quantum fields, especially holograms in QBD.

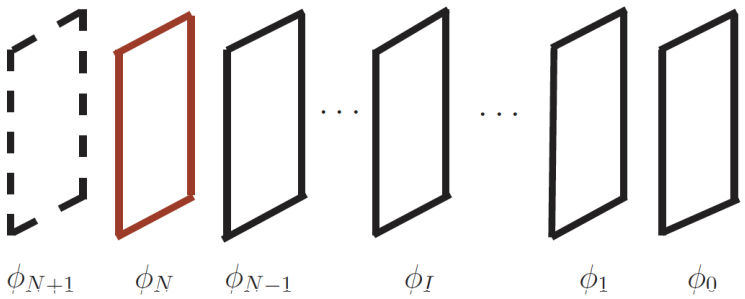

FIG. 1. Quantum field $\phi(x)$ in a hierarchy.

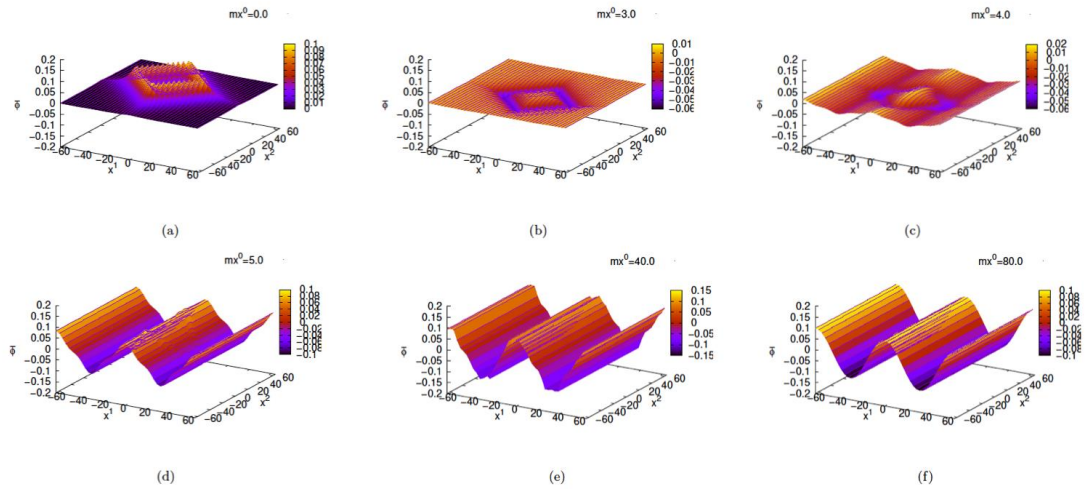

FIG. 2. Distribution of evolving coherent field $\phi(x)$.

Acknowledgement

The present work was supported also by MEXT Quantum Leap Flagship Program (MEXT QLEAP) Grant Number JPMXS0120330644.

Reference

[1] Akihiro Nishiyama, Shigenori Tanaka, and Jack A. Tuszynski. Non-equilibrium Quantum Brain Dynamics II: Formulation in 3+1 dimensions. Physica A: Statistical Mechanics and its Applications, 567:125706, 2021.

[2] Akihiro Nishiyama, Shigenori Tanaka, and Jack A. Tuszynski. Quantum Brain Dynamics and Holography. Dynamics 2.2: 187-218, 2022.

SE-03B-α2-03

Construction of dipeptide-based DNP-NMR molecular probe library focusing on kidney injury mouse model

Yuki Aketa[1], Yutaro Saito[1], Fuminori Hyodo[2], Masayuki Matsuo[3] and Shinsuke Sando[1,4]

[1]*Department of Chemistry and Biotechnology, Graduate School of Engineering, The University of Tokyo, Japan*

[2]*Department of Radiology, Frontier Science for Imaging, School of Medicine, Gifu University, Japan*

[3]*Department of Radiology, School of Medicine, Gifu University, Japan*

[4]*Department of Bioengineering, Graduate School of Engineering, The University of Tokyo, Japan*

Introduction

Dissolution dynamic nuclear polarization (dDNP) is a powerful technique that dramatically enhances the sensitivity of molecular probes in nuclear magnetic resonance imaging (NMR/MRI), which allows non-invasive detection of NMR/MRI signals in a deep site of the body with high sensitivity[1,2]. Molecular probes hyperpolarized with dDNP have been successfully applied for metabolic imaging *in vivo* and have been expected to have medical applications such as disease diagnosis and assessment of drug treatment[2,3]. Although various DNP-NMR molecular probes have been developed[4], a limited number of biomarkers, usually well-studied enzymes, have been targeted despite the enormous number of potentially targetable enzymes expressed *in vivo*. This situation is mainly due to the paucity of enzymes known to be associated with diseases. In addition, it is unclear which enzymatic activity is applicable to the diagnosis of diseases by DNP-MRI even if the enzymatic activity can be detected in the biosamples. To expand the utility of DNP-NMR, it is desired to devise a new approach to discover biomarker enzymes applicable to the disease diagnosis by DNP-NMR. To this end, we envisioned that it would be an effective strategy to compare the metabolic activity of diseased and healthy tissues for a compound library and discover molecules with disease-specific activity. We focused on exopeptidase which cleaves *N*- or *C*-terminus peptide bonds in peptides because they are known to be related to disease progression,[5-7] and we selected dipeptides for the library because they could be recognized from two types of exopeptidases, aminopeptidase and carboxypeptidase, at least.

In the present study, we designed dipeptide libraries targeting aminopeptidases and carboxypeptidases respectively and prepared 180 compounds of the dipeptide libraries in total. Finally, we carried out a screening assay with the dipeptide libraries in the kidney injury mouse model. In this presentation, we will show the design strategy for the dipeptide libraries and the screening results.

Tables and Figures

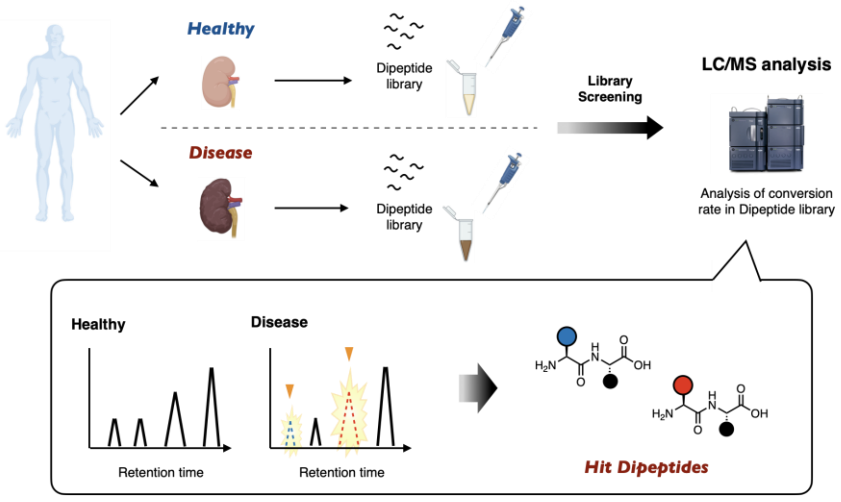

Figure. 1. Strategy for discovering new biomarkers in this study.

Reference

[1]J. H. Ardenkjær-Larsen *et al.*, *Proc. Natl. Acad. Sci. U. S. A. 100*, 10158–10163 (2003).

[2]K. Golman *et al.*, *Proc. Natl. Acad. Sci. U. S. A. 103*, 11270–11275 (2006).

[3]S. E. Day *et al.*, *Nat. Med. 13*, 1382–1387 (2007).

[4]Y. Kondo *et al.*, *Angew. Chem. Int. Ed. 60*, 2–23 (2021).

[5]L. Guzman-Rojas *et al.*, *Proc. Natl. Acad. Sci. U. S. A. 109*, 1637–1642 (2012).

[6]D. A. Silver *et al.*, *Clin. Cancer Res. 3*, 81–85 (1997).

[7]P. Selvakuamar *et al.*, *Clin. Cancer Res. 10*, 2771–2775 (2004).

This work was supported by MEXT Quantum Leap Flagship Program (MEXT Q-LEAP) Grant Number JPMXS0120330644.

SE-03B-α2-04

Nuclear hyperpolarization of liquid water by using photoexcited triplet electrons in organic nanocrystals

Naoto Matsumoto[1], Koki Nishimura[1], Nobuo Kimizuka[1], Yusuke Nishiyama[2,3], Kenichiro Tateishi[4], Tomohiro Uesaka[4], Nobuhiro Yanai[1,5]

[1]*Department of Applied Chemistry, Graduate School of Engineering, Center for Molecular Systems, Kyushu University,*

[2]*NanoCrystallography Unit, RIKEN-JEOL Collaboration Center,* [3]*JEOL RESONANCE Inc.,*

[4]*Cluster for Pioneering Research, RIKEN, RIKEN Nishina Center for Accelerator-Based Science,*

[5]*FOREST, JST*

yanai@mail.cstm.kyushu-u.ac.jp

Introduction

Nuclear magnetic resonance (NMR) and magnetic resonance imaging (MRI) are powerful methods to analyze molecular structures and diagnose diseases. However, the sensitivity of NMR/MRI is quite low because of the low nuclear spin polarization. Dynamic nuclear polarization (DNP) can improve the sensitivity of NMR/MRI by transferring highly polarized electron spins to nuclear spins. On the other hand, the DNP using radical electrons uses electron polarization in thermal equilibrium, which requires cryogenic temperatures (~4 K) to obtain high polarization.

Recently, DNP using photoexcited triplet electrons (triplet-DNP) has attracted much attention (FIG. 1).[1] In triplet-DNP, the use of non-equilibrium electron polarization allows nuclear hyperpolarization even at room temperature. However, polarizable targets have been limited to solid samples because polarization transfer from electrons to nuclei requires strong dipole interactions.[2] Towards the biological application, the hyperpolarization of liquid water has remained an important challenge. In this work, we demonstrated the first hyperpolarization of liquid water by triplet-DNP.[3]

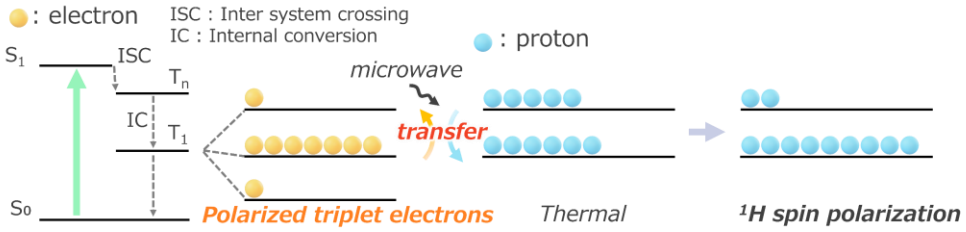

FIG. 1. Schematic representation of triplet-DNP.

Results and discussion

The hyperpolarization of liquid water in triplet-DNP requires polarization transfer from crystals to water, and it is important to increase the surface area of crystals. We prepared 3 sizes of nanocrystals, 390, 270, and 170 nm, respectively, by reprecipitation method and each sample was named NC_{390}, NC_{270}, and NC_{170}, respectively. Triplet-DNP experiments with mixtures of nanocrystals and water showed ^{1}H-NMR signal enhancement not only crystals but also water (FIG. 2a). ^{1}H-NMR enhancement of water was increased by decreasing the size of nanocrystals, indicating that hyperpolarization of water was derived from nanocrystals (FIG. 2b). Some control experiments and simulations revealed a scenario of water hyperpolarization in which polarization of photoexcited triplet electron was transferred to nuclear spins in the nanocrystals, and then transferred to liquid water at the nanocrystals-water interfaces.

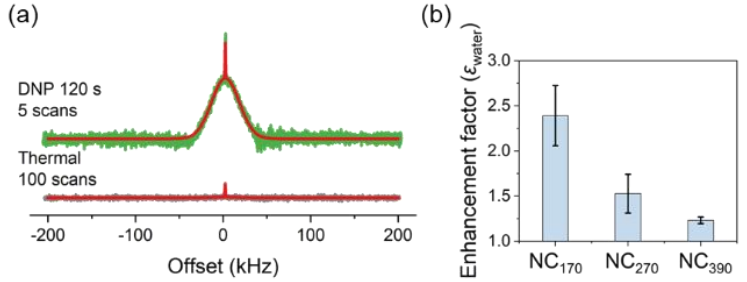

FIG. 2. (a) ^{1}H-NMR spectra of thermal (black) and after triplet-DNP for 120 s (green) at 28.2 MHz. (b) Nanocrystal size dependent ^{1}H-NMR enhancement of water.

Reference

[1]A. Henstra *et al.*, *Chem. Phys. Lett.*, **165**, 6 (1990).
[2]K. Nishimura *et al.*, *Chem. Commun.*, **56**, 7217 (2020)
[3]N. Matsumoto *et al.*, *J. Am. Chem. Soc.*, **144**, 18023 (2022)

SE-03B-α2-05

Development of Polarizing Agent with Controlled Electronic Structure for Highly Efficient triplet-DNP

Keita Sakamoto[1], Tomoyuki Hamachi[1], Kenichiro Tateishi[2], Tomohiro Uesaka[2], Nobuo Kimizuka[1,3], Nobuhiro Yanai[1,3,4]

[1]*Department of Applied Chemistry, Graduate School of Engineering, Kyushu University*

[2]*RIKEN Nishina Center for Accelerator-Based Science*

[3]*Center for Molecular Systems (CMS) Kyushu University*

[4]*FOREST, Japan Science and Technology Agency*

yanai@mail.cstm.kyushu-u.ac.jp

Introduction

Dynamic nuclear polarization using photo-excited triplet electron (triplet-DNP) achieves the nuclear hyperpolarization by transferring polarization from triplet electron spins to nuclear spins. However, it has remained difficult to attain large nuclear polarization in amorphous materials of practical importance. This is due to the broadening of ESR spectra of the triplet state by the random orientation of the polarizing agents and the anisotropic interaction of the electron spins. While the ESR spectra can be sharpened by controlling the orientation of the polarizing agents within a single crystal,[1,2] the target molecules cannot be incorporated into the single crystal. Therefore, instead of such "orientation control", this study aims to sharpen the ESR spectra and improve the DNP efficiency by "molecular design" focusing on the electronic structure of polarizing agents.

Method

The shape of the ESR spectra is determined by the zero-field splitting parameters (*D*, *E*), which reflect the electronic structure of the excited triplet state. When the electrons are symmetrically delocalized, the values of |*D*| and |*E*| become smaller and the ESR spectrum becomes sharper. In order to obtain such delocalized electronic structures, we have synthesized 6,13-di(thiophen-2-yl)pentacene) (DTP) by introducing a thienyl group, a five-membered ring with small steric hindrance, into pentacene, and evaluated its electronic structure and polarization performance (FIG 1).

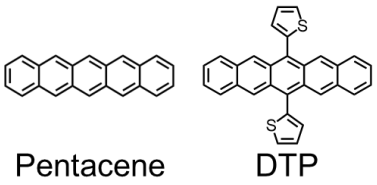

FIG. 1 Chemical structures of pentacene and DTP

Time-resolved ESR measurements of pentacene and DTP were conducted in a *β*-estradiol glass matrix. Compared to pentacene, DTP showed more intense and sharper ESR signal thanks to their smaller |*D*| and |*E*| values (FIG. 2a).

The triplet-DNP experiment was conducted with an integrated solid effect sequence. *o*-Terphenyl (OTP*h*) was employed as the amorphous matrix. FIG. 2b shows the buildup curve of ^{1}H NMR signal intensity after triplet DNP at 120 K. For triplet-DNP with DTP, the final polarization after 5 min reached 0.83%, about three times higher than that with pentacene. Triplet-DNP of partially deuterated OTP ([D_{14}]OTP : OTP = 90 : 10 wt% (OTP*d*)) with DTP resulted in the polarization of 7.5%,which was much higher than the previous highest value of 1.5%.[3]

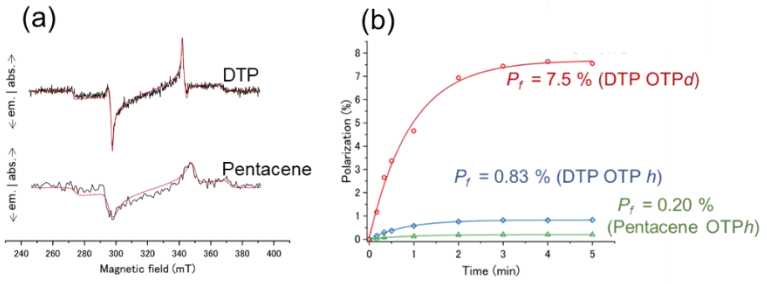

FIG. 2 (a) ESR spectra and, (b) buildup curve of ^{1}H NMR signal Intensity.

Reference

[1]Takeda. K, *Triplet State Dynamic Nuclear Polarization* (VDM, Saarbrücken, Germany, 2009).
[2]Tateishi. K, et al., *Proc. Natl. Acad. Sci. U. S. A*, 111, 7527–7530 (2014).
[3]Tateishi. K, et al., *Angew. Chem. Int. Ed,52*, 13307-13310 (2013).

SE-03B-α2-06

DNP-NMR molecular probe for the detection of Dipeptidyl peptidase-4 activity *in vivo*

Akihito Goto[1], Hiroyuki Yatabe[1], Kazutoshi Yamamoto[2], Murali C. Krishna[2], Yutaro Saito[1], and Shinsuke Sando[1]

[1]*Department of Chemistry and Biotechnology, Graduate School of Engineering, The University of Tokyo*

[2]*National Institute of Health, USA*

goto-akihito0528@g.ecc.u-tokyo.ac.jp

Introduction

Dipeptidyl peptidase-4 (DPP-4) is a peptidase that cleaves peptides at the second residues from the N-terminal terminus, preferentially when the second residue is proline or alanine (Figure 1). Because DPP-4 is related to various diseases such as type 2 diabetes and cancers, DPP-4 is a potential therapeutic target and biomarker[1,2]. Thus, the detection of DPP-4 activity *in vivo* will be a powerful technique for diagnosis.

Nuclear magnetic resonance imaging (NMR/MRI) is an imaging method that can observe and visualize the dynamics of molecular targets deep inside the body at high spatiotemporal resolution. In the medical field, however, the observation targets are limited to ^{1}H nuclei of water or lipids abundant in the body. This is due to the low sensitivity of NMR. Dynamic nuclear polarization (DNP) can solve this problem by enhancing NMR sensitivity as much as 10^{3}–10^{5} times. DNP is achieved by irradiating microwave to probes in the presence of stable radicals at a cryogenic temperature under high magnetic field to transfer polarization of electron spins to nuclear spins[3]. DNP-NMR molecular probes are required to satisfy the following requirements: (1) sufficient length of spin-lattice relaxation time correlated with hyperpolarized lifetime, (2) sufficiently large chemical shift change to distinguish a molecular probe and a product, (3) fast reaction with targets, and (4) selective reaction with targets (Figure 2).

In this study, we attempted to develop a DNP-NMR molecular probe for the detection of DPP-4 activity *in vivo* by designing the molecular structure to satisfy these requirements. In the presentation, we will show the design strategy and the recent results.

Tables and Figures

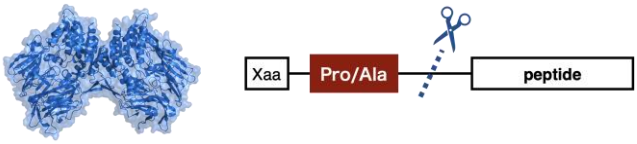

Figure 1. DPP-4 and preferential cleavage site.

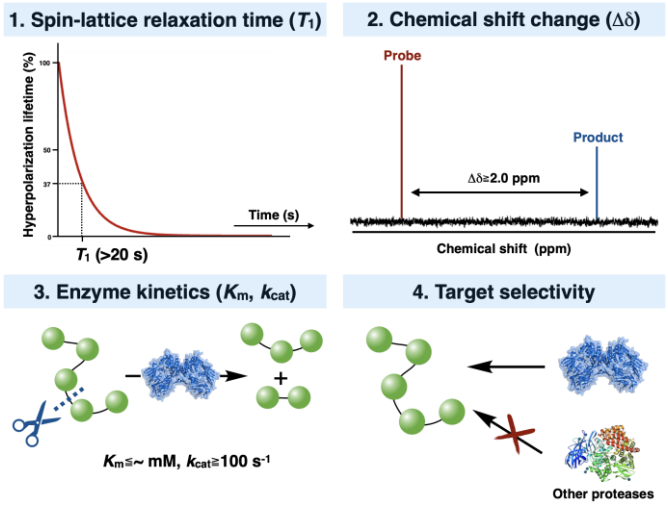

Figure 2. Requirements for DNP-NMR molecular probes.

References

[1]C. F. Decon, *Front. Endocrinol. 10*, 80 (2019).

[2]K. Ohnuma *et al.*, *Front. Biosci. 23*, 1754–1779 (2018).

[3]J. H. Ardenkjaer-Larsen *et al.*, *Proc. Natl. Acad. Sci. U. S. A. 100*, 10158‑10163 (2003).

This work was supported by MEXT Q-LEAP Grant Number JPMXS0120330644

SE-03B-α2-07

Generation of polarized triplet electron spins at solid-liquid interfaces

Reiya Yabuki[1], Tomoyuki Hamachi[1], Koki Nishimura[1], Kenichiro Tateishi[2], Tomohiro Uesaka[2] and Nobuhiro Yanai[1,3,4]

[1] *Department of Applied Chemistry, Graduate School of Engineering, Kyushu University*

[2]*RIKEN Nishina Center for Accelerator-Based Science*

[3]*Center for Molecular System, Kyushu University*

[4]*FOREST, Japan Science and Technology Agency*

yanai@mail.cstm.kyushu-u.ac.jp

Introduction

Triplet-DNP can enhance NMR sensitivity at room temperature utilizing the electron polarization of the triplet state[1,2]. However, it has been difficult to enhance the solution NMR signal by triplet-DNP due to the immediate relaxation of polarized triplet electron spins in solution. Towards the direct polarization of solution by triplet-DNP, we aim for the generation of polarized triplet electron spins at solid-liquid interfaces.

Method

In this study, we used tetrakis (4-carboxyphenyl) porphyrin (TCPP, FIG. 1a) as a polarization agent and aminopropyl silica gel (ASg, FIG. 1b) as a solid support. TCPP-modified ASg was dispersed in toluene. We evaluated whether polarized electron spins of triplet states are generated at the solid-liquid interface by time-resolved ESR measurements.

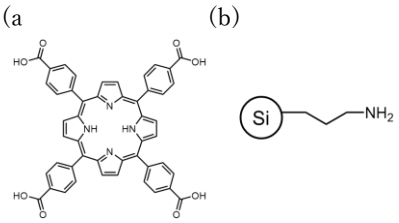

FIG. 1. Chemical structures of (a) TCPP and (b) ASg

Under pulsed laser excitation at 527 nm, ESR spectrum and the peak decay of TCPP on ASg surface in toluene were measured. The ESR spectrum showed a characteristic line shape of the spin-polarized triplet state of TCPP[3] (FIG. 2). Furthermore, the lifetime of the spin-polarized state was approximately 3.0 μs, which was long enough to carry out the triplet-DNP measurement. This result indicates that the use of solid support suppressed the dynamics of the polarization agents and the relaxation of electron spin polarization at the solid-liquid interface.

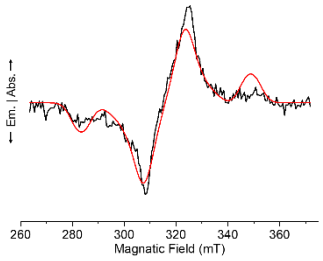

FIG. 2. ESR spectrum of TCPP-ASg in toluene

Reference

[1]W. T. Wenckebach et al., *Chem. Phys. Lett.*, 165, 6-10 (1990)

[2]N. Yanai et al., *J. Phys. Chem. Lett.*, 10, 2645-2650 (2021)

[3]L. Bolzonello et al., *Phys. Chem. Chem. Phys.*, 19, 27173-27177 (2017)

SE-03B-α2-08

Photoreaction study of a primate blue-light sensitive photoreceptor using vibrational spectroscopy

Yosuke Mizuno[1], Kota Katayama[1], Hiroo Imai[2], and Hideki Kandori[1]
[1] Graduate School of Engineering, Nagoya Institute of Technology
[2] Center for the Evolutionary Origins of Human Behavior, Kyoto University
y.mizuno.092@stn.nitech.ac.jp

Introduction

Photoreceptor proteins are expressed in eyes and function as vision systems. There are two types of photoreceptors. One is rhodopsin which responsible for twilight vision, another one is cone pigments which responsible for color vision. These proteins commonly bound 11-*cis*-retinal as a chromophore. Retinal absorb UV light (370 nm) in the solution and absorb about 440 nm by making Schiff base linkage. Further, protein moiety determines the absorption range from UV to red light[1].

The photoreaction mechanisms and structural information were well known in rhodopsin. However, Cone pigment have been less known than rhodopsin because of low expression level and handling difficulty. We previously observed the first structural data of the primary Batho intermediate state of primate red (MR), green (MG) and blue (MB) cone pigments by low-temperature FTIR spectroscopy [2]. Recently, we also reported the structural study of BL intermediate in MB which is formed from initial photointermediate [3]. Here, we extended these vibrational structural studies by identifying subsequent photointermediate of cone pigments, especially MB.

Results

By using low-temperature UV−visible spectroscopy, we found that the Lumi intermediate (223K) of MB formed in transition from the BL intermediate (163K) shows an absorption maximum in the UV region (Fig.1), indicating the deprotonation of the retinal Schiff base. Comparison of the light-induced difference FTIR spectra of Batho (77K), BL, and Lumi showed significant α-helical backbone C=O stretching (1661 and 1652 cm^{-1}) and protonated carboxylate C=O stretching vibrations (1714 and 1712 cm^{-1}) only in the Lumi intermediate (Fig.2). Thus, the transition from BL to Lumi involves dramatic changes in protein environment with a proton transfer reaction between the Schiff base and the counterion resulting in an absorption maximum in the UV region[4].

Tables and Figures

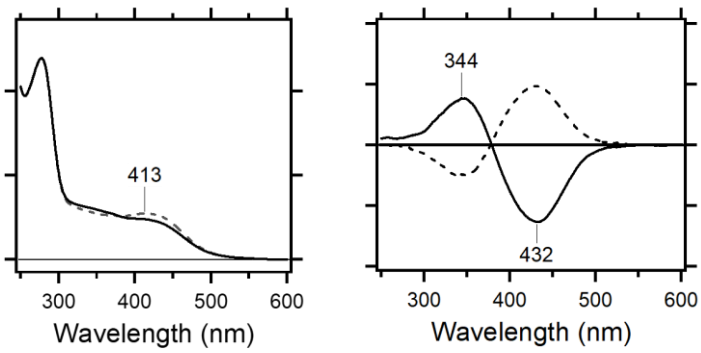

FIG.1. UV-visible absorption spectra of MB (left) and light-induced difference spectra (right) with >430 nm illumination (solid line) and 360 nm illumination (dash line) at 223K

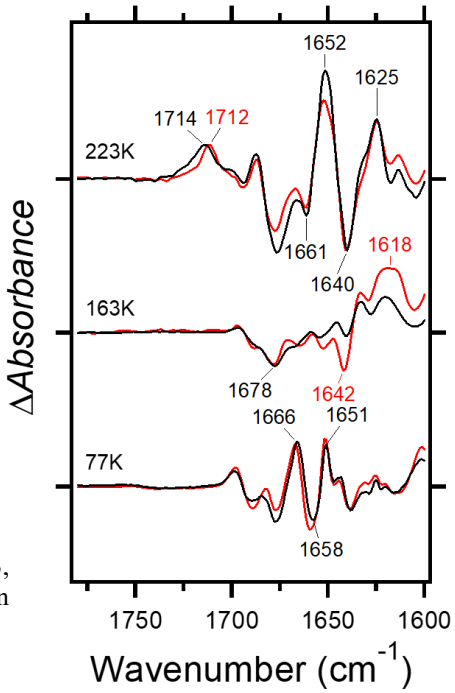

FIG.2. Light-minus-dark difference FTIR spectra of MB at 223, 163, and 77 K in the 1780−1600 cm^{-1} region. Spectra were measured in H_2O (black) and D_2O (red).

Reference

[1]O.P. Ernst et al., *Chem Rev*, 114, 126-163 (2014).
[2]K. Katayama et al., *Sci Rep*, 7, 4904 (2017).
[3]S. Hanai et al., *Biophys Physicobiol*, 18, 40-49 (2021).
[4]Mizuno et al., *Biochemistry*, in press

SE-03B-α2-09

Novel photoisomerization reaction in near-infrared light absorbing enzymerhodopsins

Masahiro Sugiura[1*], Kazuki Ishikawa[1], Kota Katayama[1,2], Yuji Sumii[1], Rei Abe-Yoshizumi[1], Satoshi P. Tsunoda[1,2], Yuji Furutani[1,2], Norio Shibata[1], Leonid S. Brown[3], Hideki Kandori[1,2**]

[1] *Department of Life Science and Applied Chemistry, Nagoya Institute of Technology, Japan*
[2] *OptoBioTechnology Research Center, Nagoya Institute of Technology, Japan*
[3] *Department of Physics and Biophysics Interdepartmental Group, University of Guelph, Canada*
*: m.sugiura.734@stn.nitech.ac.jp, **: kandori@nitech.ac.jp

Introduction

Rhodopsins is a large family of retinal-binding photoreceptive membrane proteins found in microbes and animals [1]. Microbial rhodopsins has different functional family, including light-driven ion pumps, light-gated ion channels, light sensors, and light-activated enzymes (FIG.1). Microbial rhodopsins possess retinal chromophores that capture light energy and isomerize from all-trans to 13-cis (FIG.1). Although this isomerization reaction was universally conserved in microbial rhodopsins, a recently discovered microbial rhodopsin, bestrhodopsin, offered surprising photochemical properties.

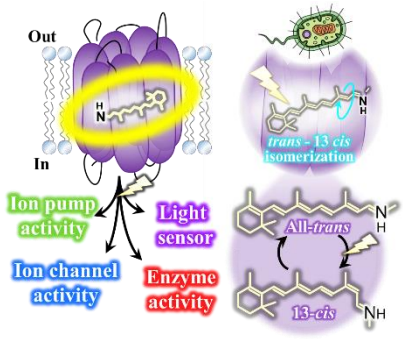

FIG.1 Functions and photoisomerization of microbial rhodopsin

Bestrhodopsin is a far-red light absorbing novel microbial rhodopsin, in which one or two rhodopsin domains are fused to a bestrophin channel and function as light-gated ion channels [2]. The surprises were that bestrhodopsin performs an all-trans to 11-cis photoisomerization and it show no photoreaction at low temperatures at <170K, despite any microbial rhodopsin can react [2].

Our target protein is enzymerhodopsin (NeoR) which was reported in 2020 [3]. This NeoR is similar to besrhodopsin in the following four points [3]. First, it absorbs far-red and near infra-red light. Second, the rhodopsin domain forms heterodimers. Third, it has eight transmembrane α-helices whereas normal rhodopsin is composed of seven transmembrane α-helices. Finally, three carboxylic acids are conserved around the retinal as a chromophore, different from normal microbial rhodopsins which have one or two carboxylic acids near the retinal. Despite these similar properties between bestrhodopsin and NeoR, the detailed photochemical properties of NeoR remained unknown.

Thus, we clarified the photochemical properties of NeoR using HPLC and spectroscopy.

Results

We studied a novel near-infrared light-absorbing enzymerhodopsin from *Obelidium mucronatum* (OmNeoR). OmNeoR show guanylyl cyclase activity upon light irradiation, when it form heterodimers. Using UV-vis spectroscopy, it is revealed that OmNeoR absorbs near infrared light, and its absorption wavelength converts the dark state into a stable UV-absorbing state.

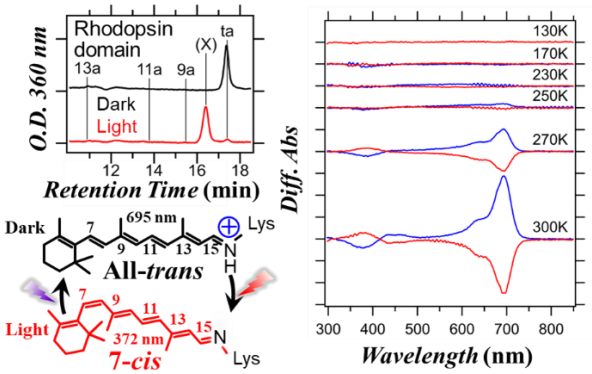

FIG.2 Retinal isomerization in NeoR and photoreaction at low temperature.

Using HPLC analysis which can determine composition ratio of retinal isomers in rhodopsin, anti-oxime peak (X) is observed different from f 13-*cis*, 11-*cis*, 9-*cis*, or all-*trans* form. In previous research, peak (X) is probably 7-cis. However, 7-cis retinal is unstable, because of a steric hindrance between the 9-methyl group and methyls in the β-ionone ring. In addition, an HPLC peak of di-cis retinal oxime, such as the 9,11-di-cis form, can appear between those of 9-cis and all-trans retinal oxime. Thus we weren't sure if peak (X) was really 7-cis form. Here, we isolate same isomer as peak (X) and measure the ^{1}H NMR spectra which is consistent with 7-cis form. Therefore, we conclude that peak (X) is 7-*cis* retinal.

In addition, OmNeoR show no photoreaction at <270K. It indicate that there exist potential barrier for 7-cis isomerization in excited state of OmNeoR.

In this presentation, we would like to discuss the unique photoisomerization reaction of NeoR.

Reference

[1]O.P. Ernst et al., *Chem Rev*, 114, 126-163 (2014).
[2]A. Rozenberg et al. *Nat. Struct. Mol. Biol*, 29, 592−603 (2022)
[3]M. Broser et al. *Nat.Commun.* 11, 5682 (2020)

SE-03B-α2-10

Development of a real-time 4D quantum temperature imaging system to measure intercellular thermal diffusivity

Haruka Maeoka[1], Ryuji Igarashi[2], Shin Usuki[3], and Takuma Sugi[1]

[1]*Program of Biomedical Science, Graduate School of Integrated Sciences for Life, Hiroshima University*

[2] *Quantum Science and Technology Organization*

[3] *Research Institute of Electronics, Shizuoka University*

m211518@hiroshima-u.ac.jp

Cellular function is severely affected by temperature change. Heat produced within a cell controls its own cellular function cell-autonomously and neighboring cells' function non-cell-autonomously. While several studies have focused on intracellular thermal diffusion, few have reported on how intercellular thermal diffusion influences neighboring cells' function. This question could be addressed by estimation of the intercellular thermal diffusivity, which requires quantifications of temperatures at three-dimensionally distributed multiple cells during thermal diffusion. However, assuming that the thermal diffusivity in cells is the same as that in water, 1.5×10^{-7} m^2 / sec, it takes 1 millisecond for heat to diffuse through multiple 10 μm cells in all XYZ directions. In contrast, when we take images using a 100 fps camera with 100 scans along Z-axis and 30 times data accumulations, current 3D imaging technologies such as confocal microscopy take 50 milliseconds to measure temperature of multiple cells along Z-axis. This means that the measurement speed of the current technologies is insufficient to observe 3D intercellular heat diffusion which completes within 1 millisecond.

Recently, we developed the high-resolution light field microscopy (HR-LFM) capable of 'scan-less' 3D imaging by capturing 3D space as a 2D image using a micro-lens array. We also focused on the fluorescent nanodiamonds (FNDs) which allow for highly sensitive temperature measurement. Here, these two cutting-edge technologies inspired us to establish a system for measuring the temperatures of multiple cells with an acquisition rate faster than heat diffusion rate. First, (1) we constructed a 'selective imaging' system to selectively extract the fluorescence of only FNDs from among background fluorescence by irradiating microwave that induces electron spin resonance to modulate the fluorescence of FNDs. Then, we synchronized 'scan-less' 3D detection of multiple signals by HR-LFM with microwave irradiation. This enabled simultaneous selective extraction of multiple FNDs' fluorescence from among fluorescent beads in a 3D sample and from among an autofluorescence in *C. elegans*, thereby achieving 3D selective imaging 50-fold faster than confocal microscopy. Second, (2) we attempted to establish the system for measuring 3D heat diffusion. We successfully measured temperature changes at multiple 3D locations simultaneously in nematode *C. elegans*, thus achieving 3D temperature imaging 100-fold faster than confocal microscopy. Using this method, we will calculate the intercellular thermal diffusivity by measuring the intercellular heat diffusion from a heat source cell to neighboring cells *in vivo*.

SE-03B-α2-11

Bidirectional neural network and its application to image denoising, super-resolution, and image completion

Kei Majima[1,2], Noriaki Yahata[1]

[1]*Institute for Quantum Life Science, National Institutes for Quantum Science and Technology (QST), Chiba, Japan*

[2]*PRESTO, Japan Science and Technology Agency (JST), Japan*

majima.kei@qst.go.jp

Introduction

Quantum sensing technology has enabled the development of new methods to visualize various physical parameters of interest in biological systems. For example, the concentration of specific molecules can be visualized by magnetic resonance imaging (MRI), and an electromagnetic field or distribution of temperature can be reconstructed by nitrogen-vacancy center sensing (NV-center sensing). Because observed image data are sometimes noisy/low-resolution/incomplete, image processing to recover clean/high-resolution/complete images from the observed ones is a critical step that must be developed. In this report, we present a unified framework for the above-mentioned image-processing tasks using neural networks.

Methods

We describe our proposed framework by taking the super-resolution task as an example. Note that the same framework can also be used for image denoising and image completion. In our framework, we assume that a set of low-resolution images and the corresponding high-resolution images are available as training data. Then a bidirectional neural network, which is a neural network whose each layer is bidirectional, is trained using the training data (Fig 1A). Following the neural network training, for new low-resolution images, the corresponding high-resolution images can be estimated using this neural network as a converter.

Results

Using two types of toy image data, we tested the proposed framework on three types of image-processing task: 1) image denoising, 2) super-resolution, and 3) image completion. Results of the super-resolution task are shown in Fig. 1B and C.

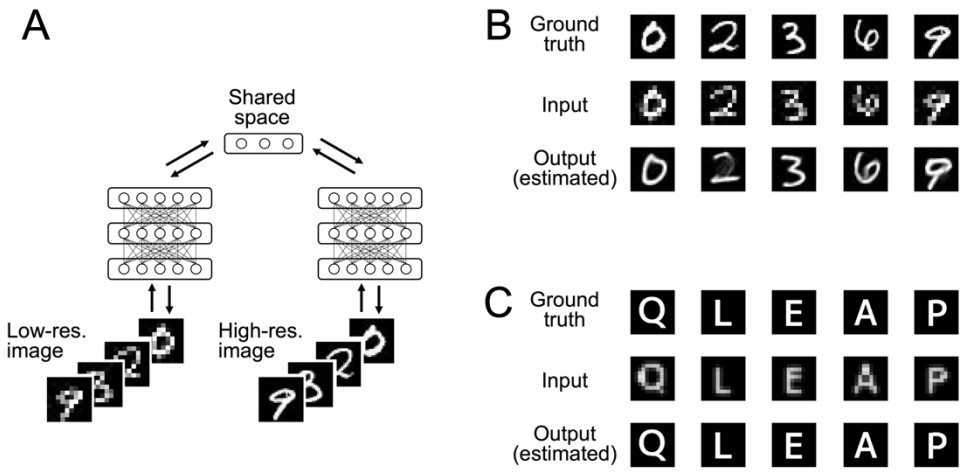

FIG 1. Neural network-based image-preprocessing framework. A schematic of neural network training (panel A) and results of the super-resolution task (panels B,C) are shown.

Discussion and Conclusions

In this report, we presented an image-processing framework using a bidirectional neural network, and our preliminary results showed that this framework can effectively perform several types of image-processing task. The application to real experimental data in the field of quantum sensing will be addressed in our future studies.

Acknowledgments

This research was supported by MEXT Q-LEAP (JPMXS0120330644), JSPS KAKENHI (20K16465), JST ERATO (JPMJER1801), and JST PRESTO (JPMJPR2128).

SE-03B-α2-12

Molecular insight into photoactivation mechanism of BLUF protein by QM/MM free energy simulation

Masahiko Taguchi, Shun Sakuraba, Justin Chan, and Hidetoshi Kono
Institute for Quantum Life Science, National Institutes for Quantum Science and Technology
taguchi.masahiko@qst.go.jp

Introduction

OaPAC is a photoactivated enzyme that forms a homodimer [1,2]. It has two BLUF photoreceptor domains connected to the catalytic domains via long coiled-coil C-terminal helixes. It is thought that during photoactivation, reorganization of hydrogen bonding network between Tyr6, Gln48, and chromophore and keto-enol tautomerization of Gln48 occur in the BLUF domain [3,4]. However, the free-energy profile of the photo-isomerization reaction and how the structural change in the BLUF domain propagates toward the catalytic domain have not been revealed yet.

Method

We first focused on the BLUF domain dimer with the C-terminal helixes from the dark state X-ray crystallographic structure of OaPAC [1]. We free-energetically optimized the dark state structure using QM/MM RWFE-SCF method [5]. We considered two possible light state structures that were free-energetically optimized. The free-energy differences between the dark and two light state structures were evaluated by the free-energy perturbation calculation. To clarify differences in protein dynamics upon photo-isomerization, we performed long-time MD simulations for the dark and light state structures.

Results

The free-energy difference between the two light state structures was estimated ~4.7 kcal/mol. The light state model with a lower free energy is consistent with a FTIR experiment result [4], but is inconsistent with light state X-ray crystallographic structure [2] in the assignment of nitrogen and oxygen atoms of Gln48 sidechain. Our component analysis of free-energy difference between the dark and light state structures showed that the chemically unstable enol tautomer of Gln48 in the light state is stabilized by a strong hydrogen bonding network with chromophore and Tyr6. Moreover, in the light state, we observed a flip of Trp90 nearby the C-terminal helix, causing the subsequent structural changes in the BLUF core and the C-terminal helix.

This work was supported by MEXT Q-LEAP Grant Number JPMXS0120330644.

References

[1] M. Ohki *et al.*, Proc. Natl. Acad. Sci. USA **113**, 6659 (2016).
[2] M. Ohki *et al.*, Proc. Natl. Acad. Sci. USA **114**, 8562 (2017).
[3] T. Domratcheva *et al.*, Sci. Rep. **6**, 22669 (2016).
[4] T. Iwata *et al.*, J. Am. Chem. Soc. **140**, 11982 (2018).
[5] S. Hayashi *et al.*, Annu. Rev. Phys. Chem. **68**, 135 (2017).